



Published
for the
International
Glaciological
Society

THIS MANUSCRIPT HAS BEEN SUBMITTED TO THE JOURNAL OF GLACIOLOGY AND HAS NOT BEEN PEER-REVIEWED.

Multi-temporal elevation changes of Fedchenko Glacier (Tajikistan) from 1928 to 2021

Journal:	<i>Journal of Glaciology</i>
Manuscript ID	Draft
Manuscript Type:	Article
Date Submitted by the Author:	n/a
Complete List of Authors:	Brun, Fanny; Institut des Geosciences de l'Environnement, IRD Lambrecht, Astrid; Bavarian Academy of Sciences and Humanities, Geodesy and Glaciology Mayer, Christoph; Bavarian Academy of Sciences and Humanities, Geodesy and Glaciology Rezaei, Janali; Institut des Geosciences de l'Environnement, IRD Dehecq, Amaury; IGE, Beraud, Luc; Institut des Géosciences de l'Environnement, Deschamps-Berger, César; Pyrenean Institute of Ecology-CSIC, Jaca, Spain Berthier, Etienne; Université de Toulouse, LEGOS (CNES/CNRS/IRD/UT3) Voelksen, Christof; Bavarian Academy of Sciences and Humanities, Geodesy and Glaciology KAYUMOV, Abdulkhamid; Center for Research of Glaciers of the National Academy of Sciences of the Tajikistan
Keywords:	Glacier mass balance, Glacier surges, Laser altimetry, Mountain glaciers
Abstract:	The Fedchenko Glacier in Tajikistan's central Pamir region is one of Asia's longest glacier and has been a focal point for scientific investigation spanning the 20th and 21st centuries, yielding a valuable historical dataset for Central Asia. This study explores elevation changes from 1928 to 2021 from topographic maps from 1928 and 1958, KH-9 spy satellite data from 1980, SPOT5 satellite data from 2011, and Pléiades satellite data from 2017, 2019, and 2021, along with GNSS surveys for absolute

	<p>co-registration. The 93-year mean rate of elevation change is -0.46 m yr^{-1}. Notably, the tongue's thinning rate is twice as negative as the long-term average in two sub-periods (1958-1980 and 2010-2021), possibly linked to a surge-like event for the earlier period. Analyses of ERA5 reanalysis (1950-2021) and Fedchenko meteorological station data (1936-1991) reveal a dry anomaly in 1958-1980 followed by a wet anomaly in 1980-2010, potentially offsetting temperature-induced mass losses. The contemporary thinning rates align with a broader trend of generalised mass losses in the Pamir region.</p>

SCHOLARONE™
Manuscripts

Multi-temporal elevation changes of Fedchenko Glacier (Tajikistan) from 1928 to 2021

Fanny BRUN,¹ Astrid LAMBRECHT,² Christoph MAYER,² Janali REZAEI,¹ Amaury DEHECQ,¹ Luc BERAUD,¹ César DESCHAMPS-BERGER,³ Etienne BERTHIER,⁴ Christof VÖLKSEN², and Abdulkhamid KAYUMOV⁵

¹*Univ. Grenoble Alpes, IRD, CNRS, INRAE, Grenoble INP, IGE, 38000 Grenoble, France*

²*Bavarian Academy of Sciences and Humanities, Munich, Germany*

³*Pyrenean Institute of Ecology-CSIC, Jaca, Spain*

⁴*Université de Toulouse, LEGOS (CNES/CNRS/IRD/UT3), Toulouse, France*

⁵*Center for Research of Glaciers of the National Academy of Sciences of the Tajikistan*

Correspondence: Fanny Brun <fanny.brun@univ-grenoble-alpes.fr>

ABSTRACT. The Fedchenko Glacier in Tajikistan's central Pamir region is one of Asia's longest glacier and has been a focal point for scientific investigation spanning the 20th and 21st centuries, yielding a valuable historical dataset for Central Asia. This study explores elevation changes from 1928 to 2021 from topographic maps from 1928 and 1958, KH-9 spy satellite data from 1980, SPOT5 satellite data from 2011, and Pléiades satellite data from 2017, 2019, and 2021, along with GNSS surveys for absolute co-registration. The 93-year mean rate of elevation change is -0.46 m yr^{-1} . Notably, the tongue's thinning rate is twice as negative as the long-term average in two sub-periods (1958-1980 and 2010-2021), possibly linked to a surge-like event for the earlier period. Analyses of ERA5 reanalysis (1950-2021) and Fedchenko meteorological station data (1936-1991) reveal a dry anomaly in 1958-1980 followed by a wet anomaly in 1980-2010, potentially offsetting temperature-induced mass losses. The contemporary thinning rates align with a broader trend of generalised mass losses in the Pamir region.

27 INTRODUCTION

28 Due to heavy irrigation and high domestic water demand in the Amu Darya basin, the Pamir mountains
29 play a crucial role for downstream freshwater supply (Immerzeel and others, 2020). The Amu Darya basin
30 contains more than 10,000 km² of glaciers, that provide around 5.5 ± 1.9 Gt of meltwater every year
31 (Pritchard, 2019; Miles and others, 2021). Glaciers lost less mass in this region in the beginning of the
32 twenty-first century, compared both with high mountain Asia and global averages (Gardelle and others,
33 2013; Lin and others, 2017; Brun and others, 2017; Shean and others, 2020; Hugonnet and others, 2021).

34 There is a large temporal gap in ground-based glacier monitoring in Central Asia following the collapse
35 of the Union of Soviet Socialist Republics (USSR). Most scientific activities in this region were abandoned
36 in the 1990s, with some of them being re-established in the past years (Hoelzle and others, 2017). This
37 gap is being partially filled in the north-western Pamir (Pamir Alay) by the re-interpretation of firn cores
38 and profiles collected in the 1970s, combined with modelling of glacier mass balance (Barandun and others,
39 2015; Kronenberg and others, 2021, 2022). In the eastern Pamir, the mass balance of Muztag Ata No.
40 15 Glacier was reconstructed from 1980 to 2017 (Zhu and others, 2018; Bhattacharya and others, 2021).
41 In the Tien Shan mountains of Kyrgyzstan, a comparison of historical and recent firn cores established a
42 reconstruction of the surface mass balance in the accumulation area of Grigoriev ice cap (Machguth and
43 others, 2024). All these studies found a tendency to increased accumulation on glaciers during the last 40
44 to 60 years together with an increased melt, that explain relatively stable mass balance in the region (Zhu
45 and others, 2018; Kronenberg and others, 2021; Machguth and others, 2024).

46 Still, in the western Pamir data remain scarce. Scientific activities focused on the longest mountain
47 glacier in the region: Fedchenko Glacier (now called Vanjyakh; 660 km², approx. 69 km long from Jasgulem
48 pass to the front), located in Tajikistan. The long-term mass balance of the glacier was calculated for the
49 period 1928-2000 (Lambrecht and others, 2014) and 1975-1999 (Zhou and others, 2019). However, these
50 studies are limited by the lack of high quality topographic data in the upper part of the glacier area, that
51 are hampered by penetration issues for the X and C-band radar data (Rignot and others, 2001; Dehecq
52 and others, 2016; Lambrecht and others, 2018) and by saturation issues for the optical data, leading to
53 incomplete coverage. GNSS data partially compensate these disadvantages, thanks to their high precision,
54 but they are not acquired frequently and provide only a partial coverage, being thus difficult to compare
55 to raster data.

56 In this study, we re-visit topographic data from 1928 and 1958 acquired by the Russian-German expe-
57 dition of 1928 and by the Academy of Sciences of the Uzbek Republic expedition of 1958 (Lambrecht and
58 others, 2014, and references therein). We combine these data with a digital elevation model (DEM) derived
59 from KH-9 imagery from August 1980, a SPOT5 DEM from November 2011, Pléiades DEMs acquired in
60 fall 2017, summer and fall 2019, and fall 2021, ICESat data from fall 2003 and GNSS data from August
61 2009, 2015, 2016 and 2019. The series of glacier elevation change is then analyzed in light of temperature
62 and precipitation changes from weather station data and reanalysis products (ERA5).

63 STUDY AREA

64 Fedchenko Glacier is one of the longest glacier in Asia, with a centerline longer than 75 km (RGI Consor-
65 tium, 2023). It is located in the central Pamir in Tajikistan. Its is fed by different accumulation basins,
66 whereof the largest one is located at the head of the main trunk, above 4 800 m a.s.l (Lambrecht and others,
67 2014). Jasgulem pass (5 300 m a.s.l.) separates the main accumulation areas of Fedchenko and Jasgulem
68 glaciers (Fig. 1). Fedchenko Gacier has multiple tributaries glaciers of various sizes, with Bivachny Glacier
69 being one of the most remarkable (Fig. 1) that is known for its past surges (Wendt and others, 2017).

70 DATA AND METHODS

71 Elevation Data

72 *Historical maps*

73 Historical maps of Fedchenko Glacier were produced by two expeditions in 1928 and 1958 (Finsterwalder
74 and others, 1932; Dittrich, 1964; Lambrecht and others, 2014) by terrestrial photogrammetry at a scale of
75 1:50 000. The maps are all based on the same local geodetic system, defined by astronomic measurements
76 during the expedition in 1928. Scans of the original maps have been orthorectified according to their original
77 projection. Then, the elevation contours and glacier boundaries have been digitised and interpolated on
78 a regular grid with a resolution of 20 m by 20 m. The errors of the final gridded elevation models are
79 estimated to less than 35 m in location and about 10 m in elevation (Lambrecht and others, 2014). Further
80 details about the map coverages and DEM generation can be found in Lambrecht and others (2014).

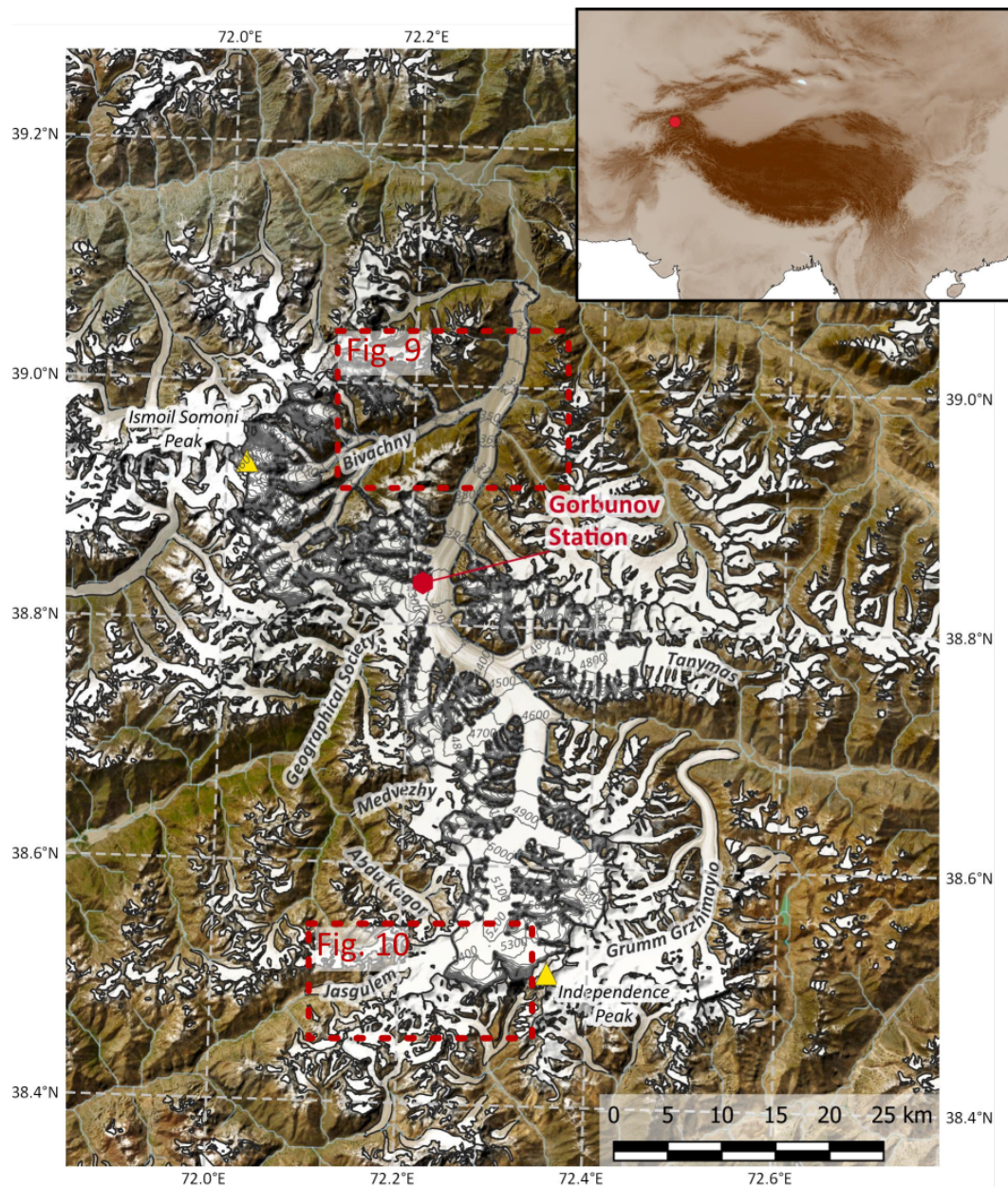


Fig. 1. Map of Fedchenko Glacier and surrounding area. The red dot on the inset map shows the location of Fedchenko Glacier. Some of the large neighbouring glaciers are named on the map. The location of Gorbunov meteorological station is highlighted, as well as the confluence with Bivachny Glacier and Jaskulem pass that are also shown of figures 9 and 10. Background image is the ESRI satellite product.

Table 1. Summary of gridded elevation data used in this study

Date of acquisition	Sensor/ Instrument	Fedchenko area covered (percent)	Vertical precision (one sigma) (m)	Comments/source
1928	Historical map	76	10	Lambrecht and others (2014)
1958	Historical map	40	10	Lambrecht and others (2014)
20 Aug. 1980	KH9	89	5	Dehecq and others (2020)
19 Nov. 2011	SPOT5	62	5	Gardelle and others (2013)
15 Oct.–23 Nov. 2017	Pléiades	73	1	Long time span
1–2 Aug. 2019	Pléiades	34	1	Upper glacier area only
28–29 Aug. 2019	Pléiades	41	1	Upper glacier area only
22–23 Sept. 2019	Pléiades	41	1	Upper glacier area only
20 Sept. 2021	Pléiades	53	1	

81 *Digital elevation models from optical satellite images*

82 In this study, we use DEMs from different types of optical images, that were all processed without ground
 83 control points (Table 1). All the elevation data are posted in the UTM 43N coordinate system and the
 84 elevations are provided relative to the WGS84 ellipsoid.

85 A pair of declassified KH-9 Hexagon images acquired on 20 August 1980 over the Pamir region was
 86 selected. This image pair is different from the image of 13 July 1975 used by Zhou and others (2019). We
 87 chose the image of 1980 because it was acquired closer to the end of the ablation season, and hence was
 88 more favourable to study glacier elevation changes. Additionally, the images from 1980 are less saturated
 89 in the accumulation basin of Fedchenko Glacier, leading to the reconstruction of a larger area compared
 90 to the images of 1975. The images were processed following Dehecq and others (2020).

91 Also, the SPOT 5 HRS DEM from Gardelle and others (2013) was included in the study. This DEM was
 92 produced by the French Mapping Agency (IGN) using correlation parameters defined during the SPIRIT
 93 (SPOT 5 stereoscopic survey of Polar Ice: Reference Images and Topographies) International Polar Year
 94 project (Korona and others, 2009). We used the DEM derived with the second set of parameters (v2), that
 95 is in principle better suited for mountainous terrain (Korona and others, 2009; Gardelle and others, 2013).
 96 Pixels with a correlation score below 75 were excluded, leading to large data voids in the accumulation area
 97 (Fig. A1). Finally, we converted the elevation provided with the Earth Gravitational Model 1996 geoid

98 (EGM96) as reference to the WGS84 ellipsoid using the *dem_geoid* command of NASA's Ames Stereo
99 Pipelines (ASP, Beyer and others, 2018).

100 In addition, we use five Pléiades DEMs from 2017, 2019 and 2021 (Table 1). The acquisitions of 2019
101 are restricted to the upper basin, and the acquisition of 2017 does not cover the lowermost section of the
102 tongue (Fig. A1). Apart from the images of early August 2019, the images are not saturated thanks
103 to the 12 bit encoding and the specific acquisition parameters (Berthier and others, 2024). The pairs of
104 images were processed using ASP. We used a semi global matching algorithm, which proved appropriate
105 for snow covered areas (Deschamps-Berger and others, 2020). Each Pléiades DEM in Table 1 was obtained
106 by stitching up to three DEMs corresponding to the respective individual Pléiades pairs that did not cover
107 the whole glacier area. In 2019, for a given date, all the scenes were acquired within two days, ensuring
108 very limited terrain changes, even over glacierized area. In 2017, the different scenes were acquired more
109 than one month apart (15 October to 23 November). However, due to the cold period and the limited
110 snowfall between the different acquisitions, we assume that changes in elevation are likely minor even on
111 the glacierized area. Thus stitching was done by co-registering the different DEMs of 2017 using a Nuth
112 and Kääb (2011) co-registration algorithm that considers the entire area covered by the DEMs (and not
113 only the off glacier terrain).

114 *ICESat data*

115 Over the whole ICESat record, there is only one track that intersected Fedchenko Glacier in fall 2003
116 (Fig. A2). ICESat footprints from the Geoscientific LASer instrument (GLAS) were converted from
117 the EGM2008 geoid to the WGS84 ellipsoid using the NSIDC GLAS Altimetry elevation extractor Tool
118 (NGAT). The nominal precision of ICESat is estimated around 0.1 m (Zwally and others, 2002). We
119 averaged the elevation of the Pléiades 2021 DEM in disks of 70 m diameter around the ICESat footprint
120 center-point and excluded the footprints with a standard deviation of elevation larger than 2 m that
121 corresponds to slopes steeper than approximately 10 degrees. After filtering, we kept 63 footprints that
122 were all acquired on 7 October 2003 (Table 2 and Fig. A2).

123 *GNSS data*

124 GNSS data were gathered during the summers of 2009, 2016, and 2019, employing various GNSS systems.
125 Initially, only GPS and GLONASS were utilized, but with the advancement of Galileo, it was integrated

Table 2. Summary of point scale data used in this study

Date of acquisition	Sensor/Instrument	Number of points	Comments
7 Oct. 2003	ICESat	63	
18–29 Aug. 2009	GNSS	9038	
7–22 Aug. 2016	GNSS	329994	
4–17 Aug. 2019	GNSS	160883	16586 points excluded

126 into the 2019 campaign. All measurements were conducted using multi-frequency systems to optimize
 127 GNSS signal utilization. The antenna was mounted on a sledge, maintaining a constant height above the
 128 surface. In 2009, the analysis relied on a local GNSS reference station on the glacier, whose coordinates
 129 were estimated using data from the nearest International GNSS Service (IGS) site. The sledge's coordinates
 130 were then computed relative to this local reference station. After 2009, Precise Point Positioning (PPP)
 131 became the method for position estimation, relying on precise clock and orbit data from GNSS satellites.
 132 This approach eliminates the need for a local reference station, simplifies fieldwork as there is no setup or
 133 maintenance required for power supply.

134 The accuracy of each position is better than 10 cm in the horizontal component and 20 cm in height,
 135 which is still a conservative estimate (Lambrecht and others, 2018). Coordinates were determined within the
 136 International Terrestrial Reference Frame (ITRF). In the first two campaigns, coordinates were referenced
 137 to ITRF2008, while the last campaign used the ITRF2014, introduced shortly before. Both reference frames
 138 exhibit negligible differences with a typical magnitude of 1 cm, which can be regarded as it is well within
 139 other source of uncertainties. The current realisations of WGS84 and various ITRFs also differ slightly in
 140 the centimetre range, as they have different originators. However, for our practical purposes, we consider
 141 them to be identical and will summarize both under the term WGS84 in the following chapters.

142 Elevation change methods

143 *Co-registration*

144 All the elevation data (i.e. GNSS and DEMs) are converted to the same spatial reference system (WGS84)
 145 and projected into UTM coordinates (43N) using ellipsoidal heights. For the DEMs derived from historical
 146 maps of 1928 and 1958, Lambrecht and others (2014) ensured the consistency between the original astro-
 147 nomical system and the WGS84 ellipsoidal elevation, which includes correcting the map elevations by a

148 32 m offset. This offset agrees well with the geoid height provided by the EGM96. Details regarding the
149 processing of the maps are available in Lambrecht and others (2014) and in references therein. The location
150 error was estimated around 35 m, and due to the limited stable terrain available, we did not apply another
151 co-registration strategy (Lambrecht and others, 2014). The DEMs from optical satellite data, calculated
152 from orbital parameters, are not perfectly georeferenced. For each of them, the horizontal and vertical
153 georeferencing can have an offset of up to dozen of meters. As a consequence, the DEMs need to be tied
154 to the GNSS data and co-registered to each other before being differentiated.

155 We first co-registered the 1-2 August 2019 Pléiades DEM on the GNSS data acquired on 4 to 17 August
156 2019. Due to the insufficient variety of slope and aspect, automatic algorithms did not perform well.
157 Instead, we manually found the horizontal displacement (x and y direction) that minimized the typical
158 aspect dependent pattern of horizontally shifted elevation products (Berthier and others, 2007; Nuth and
159 Kääb, 2011). The standard deviation of the difference between the Pléiades DEM and the GNSS points
160 is 0.41 m after excluding one spurious series of GNSS measurements (Fig. A3). We then co-registered
161 each Pléiades DEM (of 2017, 2019 and 2021) on the mosaic of 1-2 August 2019 DEM using a classical
162 co-registration algorithm (Nuth and Kääb, 2011). The 2021 Pléiades DEM covers a larger terrain, and is
163 used as a reference to co-register all the remaining DEMs that were not derived from Pléiades images.

164 *Analyzing spatially discontinuous elevation changes*

165 One of the challenges of studying the elevation changes of a glacier that has the size of Fedchenko glacier
166 is the difficulty to obtain precise elevation data that cover the whole glacier area. In particular the GNSS
167 measurements were acquired along individual profiles, and even if there are some cross overs between
168 profiles in the different years, they provide only localized elevation changes. In order to combine elevation
169 information from different spatial sampling, we apply a method inspired from ICESat processing (Kääb
170 and others, 2012). We create a 700 m wide buffer along the glacier centerline, which we split into 1 km long
171 sections along the main glacier flow, these sections are called patches hereafter (Fig. 4). We differentiate
172 all the available elevation data (DEM and GNSS) with regard to the Pléiades 2021 DEM. GNSS data
173 are differentiated with the Pléiades 2021 DEM using the *Point sampling tool* in QGIS. ICESat data are
174 differentiated with the average elevation of the Pléiades 2021 DEM in disks of 70 m diameter around the
175 footprint center-point.

For each patch and for each year i , we calculate the average elevation change relative to the 2021

DEM for each period ($\overline{dh_{i-2021}}$). For the discrete measurements (ICESat and GNSS) we do not apply any filtering. For the continuous measurements (DEMs) we consider as valid the patches with more than 40% of data coverage. For each sub-period between the years i and j , we calculate the elevation change ($\overline{dh_{i-j}}$) as:

$$\overline{dh_{i-j}} = \overline{dh_{i-2021}} - \overline{dh_{j-2021}} \quad (1)$$

176 using 2021 as the general reference level.

177 **Uncertainties on elevation changes**

178 Uncertainties on elevation changes are very difficult to quantify due to the heterogeneous sources of data
179 and the spatial averaging done here. The main sources of uncertainties on elevation changes are: i- the
180 intrinsic precision of the data, ii- the spatial sampling and iii- the temporal sampling.

181 *Intrinsic precision of the data*

182 Due to the limited stable terrain and the contrast between the rugged stable terrain and gentle glacier
183 terrain, we cannot apply standard methods to evaluate the spatial structure of variance (e.g., Rolstad and
184 others, 2009; Hugonnet and others, 2022). Instead, we report only one single metrics of DEM precision,
185 which are based on the literature (Table 1). We do not account for the effect of spatial averaging for DEM
186 differences because we investigate patches that are expected to be small with respect to the decorrelation
187 length of the DEM differences. At the scale of the patch, the errors are thus highly correlated. However,
188 when looking at a collection of patches, the spatial correlation reduces due to the distance between patches.

189 *Spatial sampling*

190 For the point-scale measurements (GNSS and ICESat), we need to test whether the measured elevation
191 changes are representative of the patch they belong to. To assess the impact of the spatial sampling, we
192 sampled the Pléiades 2017 and 2021 DEMs at the locations of each GNSS point and ICESat footprint.
193 For each patch, we average the elevation differences obtained with the GNSS or ICESat sampling, and
194 compare it with the 2017-2021 DEM difference averaged over the same patch. We find that the GNSS
195 sampling is very representative for both campaigns, with a mean difference of 0.00 m (std of 0.28 m) for
196 the 2009 GNSS campaign and 0.05 m (std of 0.34 m) for the 2016 GNSS campaign. For ICESat, we find
197 lower accuracy with a mean difference of -0.17 m and a standard deviation of 0.54 m. The difference is

198 likely due to the fact that the ICESat track intersects the side of the glacier, while the GNSS tracks follow
199 the centerline (Fig; A2).

200 *Temporal sampling - Seasonal correction of the GNSS elevations*

201 The GNSS data were acquired around mid-August (Table 2). These dates are not ideal to calculate
202 elevation changes, which should preferentially be calculated between matching dates at the end of the
203 ablation season (i.e. 1 October). The sub-annual acquisitions of Pléiades data in 1-2 August, 28-29 August
204 and 22-23 September 2019 were used to derive a correction (in m) that was applied to the GNSS data of
205 2009 and 2016 (Fig. A4). The correction is calculated as the difference between the end of September
206 DEM minus the average of the two-August DEMs, which is a proxy for a mid-August DEM. This seasonal
207 correction is available only for the upper part of the glacier, above 4500 m. It averages at -0.66 m, can be
208 as negative as -1.53 m, and has generally a higher magnitude for lower elevations, with the exception of
209 the highest locations that experienced a thinning of 0.90 m over the end of summer 2019.

210 We applied the seasonal correction to GNSS data only, because the ICESat data were acquired very
211 close to the target date of 1 October (Table 2). Regarding the DEMs, only one was acquired more than
212 one month before the end of the ablation season (the KH9 DEM of 20 Aug. 1980), but we did not apply a
213 correction as it would have a small impact on yearly change rates due to the long time spans considered.

214 **Meteorological data**

215 Meteorological data originate from two sources: the Gorbunov/Fedchenko Station (Williams and Kono-
216 valov, 2008) located at 4169 m on the eastern side of the glacier and ERA5 reanalysis data (Hersbach
217 and others, 2020). We use monthly values of temperature and precipitation from both sources. We also
218 use monthly snowfall from ERA5 reanalysis data, in order to discriminate solid and liquid precipitation.
219 Fedchenko Station operated from 1936 to 1994, providing an exceptional climate record in this data scarce
220 and remote area. ERA5 reanalysis was recently extended back to 1950, which lead to an overlap of 44 years
221 between the two records. We collected ERA5 series of temperature, precipitation and snowfall from the
222 closest grid point to the station (72.25, 38.75). It has a geopotential height of $44368 \text{ m}^2 \text{ s}^{-2}$, corresponding
223 to an elevation of 4527 m, assuming $g_0 = 9.80 \text{ m s}^{-2}$.

224 Meteorological methods

225 *Bias correction in ERA5 data*

226 Due to the height difference between the station and ERA5 grid point and the cold bias in mountainous
227 area in ERA5 (e.g., Orsolini and others, 2019; Khadka and others, 2022), we find a temperature bias of
228 -5.9 K in ERA5, relative to the Gorbunov station. After correcting for this bias, we still observe a season
229 dependent bias, with the spring/summer months being positively biased up to 1.6 K in April, and the
230 fall/winter months being negatively biased down to -2.3 K in November (Fig. A5). After removing a
231 monthly bias, the final match between ERA5 monthly temperature and the station monthly temperature
232 is very good, with a bias equal to zero, and an RMSE at 1.4 K (Fig. 2a). At annual scales, the agreement
233 between ERA5 and the station is also satisfying (Fig. 3). For the shared period, the inter annual variability
234 is slightly higher in ERA5 (0.66 K) than in the station data (0.53 K).

235 There is more dispersion in the difference between ERA5 and the station records for precipitation than
236 for temperature, with a systematic underestimation of precipitation in ERA5. We multiply the ERA5
237 precipitation by 1.9, which minimize both the RMSE and the bias between the two series (Fig. 2b). The
238 comparison shows a RMSE of 38 mm in the monthly precipitation data, but the bias between the two
239 series is limited, with a mean bias of 1 mm, which ensures that the two series can still be merged (Fig. 3).
240 Note that these statistics are calculated excluding the station data after 1990, because there is a systematic
241 negative bias in the precipitation records (Fig. A6). For the shared period, the station has a higher inter-
242 annual variability (std of 305 mm yr⁻¹) than ERA5 (std of 175 mm yr⁻¹). We apply the same factor of
243 1.9 to correct ERA5 snowfall.

244 *Temperature and precipitation anomalies*

245 We create two meteorological records named “ERA5 priority” and “station priority”, depending on which
246 dataset is used in the shared period. For the reconstructed temperature and precipitation series, the
247 anomalies are calculated on a monthly basis for the whole period (1936 until 2020). For each year, we
248 calculate the anomaly in each variable by subtracting the monthly averages over the whole period to the
249 monthly series. We also calculate annual snowfall anomalies from ERA5 record. Note that the latter are
250 calculated as percentage, and are thus unaffected by the precipitation correction factor.

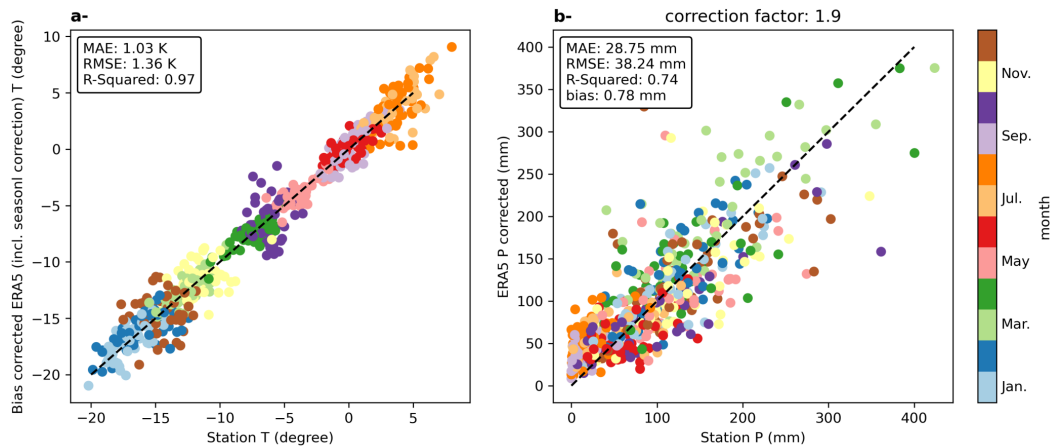


Fig. 2. Comparison of the monthly ERA5 bias corrected temperature (a) and precipitation (b) with the monthly station record for the overlapping years (1950-1994). Note that the years 1990 to 1994 were excluded for the precipitation data, due to spurious values in the station record.

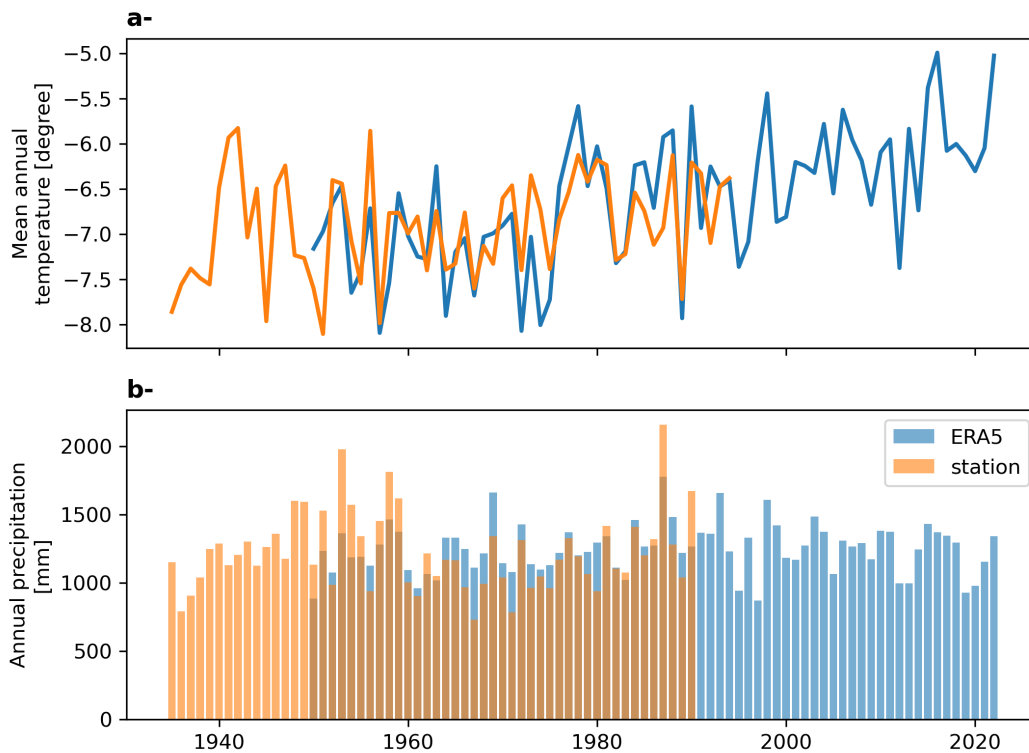


Fig. 3. Series of annual temperature (a) and precipitation (b) from ERA5 corrected and from the station record

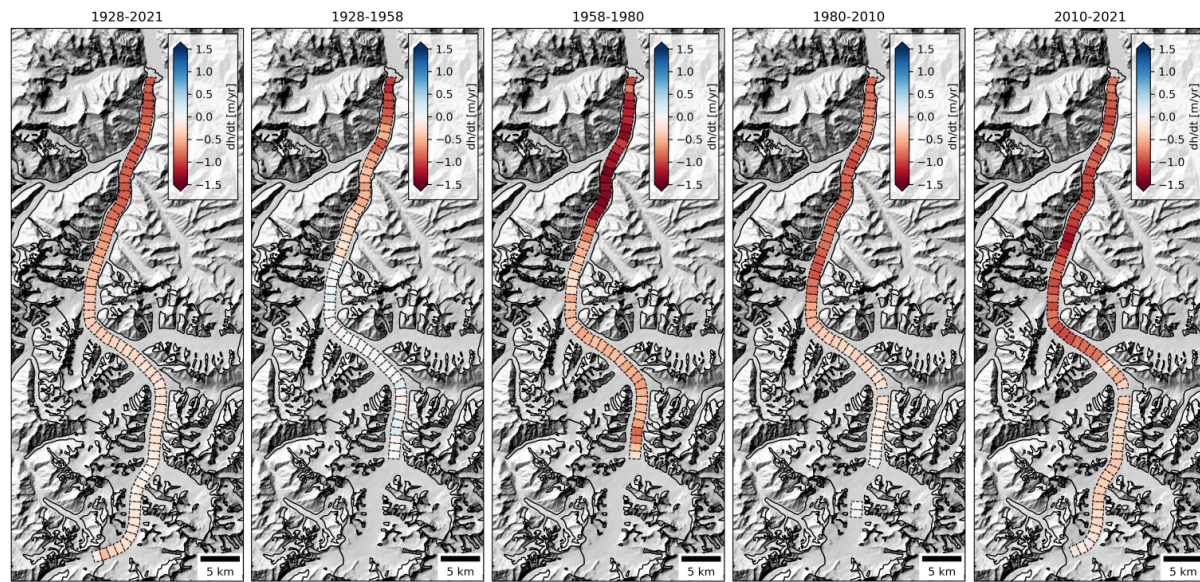


Fig. 4. Rates of elevation changes along the main trunk of Fedchenko Glacier for the different sub-periods. Background is a hillshade from the Copernicus 30 m DEM (GLO-30DEM; European Space Agency, 2022).

251 RESULTS

252 Multi-decadal elevation changes

253 For the period 1928-2021, the coverage of the glacier with elevation information is high (Table 1), especially
 254 along the central flowline that is fully covered. We observe a mean thinning rate of 0.46 m yr^{-1} , with a
 255 maximum thinning of 89.4 m (corresponding to 0.96 m yr^{-1}) roughly 4 km from the glacier front around
 256 3100 m a.s.l. (Fig. 4 and Table 3). The thinning is relatively homogeneous for the lower reaches and then
 257 decreases with elevation from approximately 80 m at 3700 m a.s.l. , to less than 10 m at 4600 m a.s.l. There
 258 is almost no elevation change detectable from 4600 to 5000 m a.s.l. (dh/dt around -0.10 m yr^{-1} ; Fig. 4
 259 and 5), but thinning increases again above 5000 m a.s.l. reaching approximately 30 m at Jasnulem pass
 260 (5250 m a.s.l.).

261 For the four sub-periods (1928-1958, 1958-1980, 1980-2010 and 2010-2021), the coverage is not always
 262 complete. For the period 1928-1958, we limit the analysis to the area below 4900 m a.s.l. , because of
 263 spurious data above this elevation (Lambrecht and others, 2014). During this 30-year period, thinning
 264 is moderate in the tongue region (-0.31 m yr^{-1}) and close to zero for most of the surveyed area located
 265 between 3700 and 4900 m a.s.l. For the period 1958-1980, we observe a marked thinning at all elevations,
 266 with a maximum thinning of -1.44 m yr^{-1} around the confluence with Bivachny Glacier. The pattern of

Table 3. Rate of elevation changes for the different sub-periods. The shared area corresponds to locations that are sampled during all sub-periods, and is thus restricted to lower reaches of the glacier. The upper area corresponds to elevations above 4 600 m a.s.l. and the lower area corresponds to elevations below 4 600 m a.s.l. For some periods the upper area is very poorly sampled and the mean elevation change is not very meaningful, these values are marked with a star (*).

Period	1928-2021	1928-1958	1958-1980	1980-2010	2010-2021
Mean dh/dt [m yr ⁻¹] - whole area	-0.46	-0.27	-0.76	-0.56	-0.69
Mean dh/dt [m yr ⁻¹] - shared area	-0.55	-0.27	-0.77	-0.59	-0.79
Max. dh/dt [m yr ⁻¹] - shared area	-0.96	-1.12	-1.44	-1.01	-1.26
Mean dh/dt [m yr ⁻¹] - lower area	-0.61	-0.31	-0.80	-0.68	-0.87
Mean dh/dt [m yr ⁻¹] - upper area	-0.18	0.02*	-0.54*	-0.07*	-0.31

267 elevation change is peculiar, as there is a rather sharp transition towards less negative rates of elevation
 268 changes seven kilometers upstream of the confluence with Bivachny Glacier. Significant thinning rates are
 269 still observed at all elevations, until the maximum observed elevation of 4900 m a.s.l. For the period 1980-
 270 2010, the glacier thinned in the lower parts (-0.68 m yr⁻¹), but slightly thickened in the main trunk from
 271 4700 to 5200 m a.s.l. It is noteworthy that the year 2010 reconstruction is a combination of the SPOT5
 272 DEM of November 2011, for elevations below 4600 m a.s.l. and of the GNSS measurements of August 2009
 273 for the upper parts (Figs. A1 and A2). For the period 2010-2021, the thinning is observed at all altitudes,
 274 with rates of elevation change around -0.87 m yr⁻¹ for the tongue, and a homogeneous elevation change
 275 rate of -0.31 m yr⁻¹ in the whole accumulation area (Fig. 4).

276 In order to compare the different sub-periods in a more quantitative way, we calculate the mean rate
 277 of elevation change over the area covered in all the sub-periods (see "shared area" in Table 3). We find an
 278 elevation change rate of -0.55 m yr⁻¹ for the period 1928-2021. The period with the most limited changes
 279 is 1928-1958, with a rate of -0.27 m yr⁻¹, while the period 1980-2010 is close to the long term average
 280 with -0.59 m yr⁻¹. The two sub-periods 1958-1980 and 2010-2021 are the most negative ones with rates of
 281 elevation changes of -0.77 and -0.79 m yr⁻¹, respectively.

282 If we compare the most recent period (2010-2021) with the earlier 82 years (1928-2010), the most
 283 striking feature is the up-glacier propagation of substantial thinning rates (> 1 m yr⁻¹) at elevations above
 284 3700 m a.s.l. (Fig. 5). In contrast, the thinning rates of the lowest parts of the glacier are very similar and
 285 average at -0.90 m yr⁻¹ below 3600 m a.s.l. for both periods. We find opposite results at the upper most

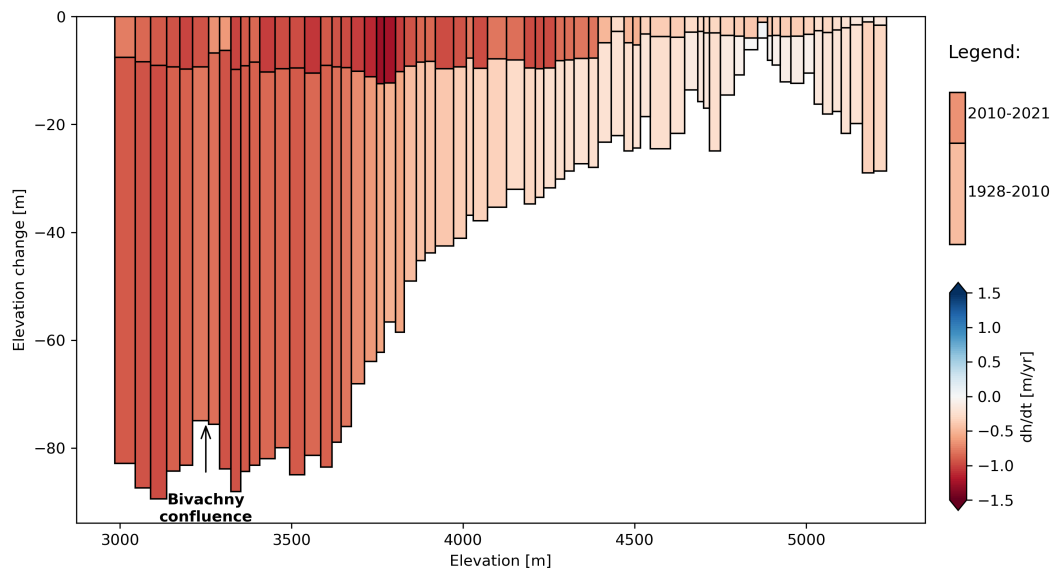


Fig. 5. Elevation changes for the periods 1928-2010 and 2010-2021 for different elevations along the centerline of Fedchenko Glacier. The bar length represents the elevation change and their color the rate of elevation change. The bar width represents the altitudinal span of each patch. The arrow shows the location of the confluence with Bivachny Glacier, and the reduced thinning due to the surge of Bivachny (Wendt and others, 2017).

286 elevations (above 5200 m a.s.l. at Jasgulem pass), where the early thinning rate of -0.32 m yr^{-1} is larger
 287 than the contemporary one at -0.13 m yr^{-1} .

288 **2003-2021 elevation changes**

289 Short term elevation changes are available only for the accumulation basin, and are based largely on
 290 ICESat, GNSS data, and Pléiades DEMs (Fig. 6). The 2003-2009 period coverage is limited, because it
 291 is based on a single ICESat track from 7 October 2003, despite a good coverage from the GNSS in 2009
 292 (Fig. A2). It is also noteworthy that ICESat sampling represents less accurately the spatial variability (see
 293 method section). Still, we observe significant thinning, ranging from -0.57 to -0.28 m yr^{-1} in the upper
 294 accumulation basin from 2003 to 2009. This period is followed by a period (2009-2016) of more moderate
 295 thinning, that averages at -0.21 m yr^{-1} . The last period (2016-2021) is the most spatially contrasted, with
 296 areas of strong thinning (-0.82 m yr^{-1}) and areas of thickening up to 0.16 m yr^{-1} (Fig. 6).

297 It is difficult to compare the three sub-periods, because of the limited spatial coverage for the period
 298 2003-2009. However, the mean rate of elevation change is roughly twice as negative for the period 2016-
 299 2021, than for the period 2009-2016, with mean rates of elevation changes of -0.41 and -0.21 m yr^{-1} ,

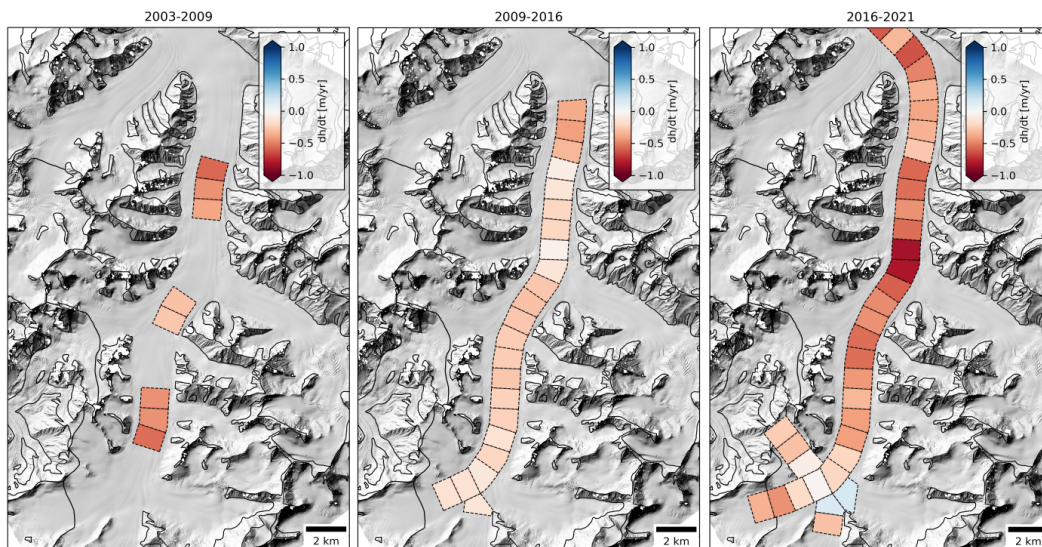


Fig. 6. Rates of elevation changes for three sub-periods in the higher part of Fedchenko Glacier from 2003 to 2021.

300 respectively. The thickening pattern for the period 2016-2019 is a robust pattern, also visible in the 2015
 301 GNSS data (not shown here, because the coverage is scarce). There is little dependency of the elevation
 302 change with elevation. For instance, the maximum thinning rate for the period 2016-2021 is located at 4900
 303 m a.s.l. For the period 2009-2016 the rate of elevation change is slightly higher for the lower elevations,
 304 but differences are still rather small.

305 Overall, the accumulation basin of Fedchenko Glacier has thinned at a substantial rate since 2000,
 306 but it is difficult to quantify the magnitude of these changes and their acceleration. The recent rates of
 307 elevation changes (2010-2021) are more negative than the long term trend (1928-2010), with the exception
 308 of Jasgulem pass, where most of the changes happened before 2010.

309 Meteorological changes

310 Both reconstructed time series show a continuous increase in temperature (Fig. 7), reaching an annual
 311 temperature anomaly of 0.60 K for the period 2010-2021, with respect to the period 1936-2021. Regarding
 312 precipitation, the year-to-year variability is large (Fig. 7). In both reconstructed records, there is a positive
 313 precipitation anomaly from 1980 to 2010 of 5 to 7 %. Additionally, in the “station priority” record, the
 314 period 1958-1980 corresponds to a dry anomaly, with a 10 % precipitation deficit, but this is not visible in
 315 the “ERA5 priority” record, which shows only a moderately negative precipitation anomaly for this period
 316 (Fig. 7). The snowfall at ERA5 grid point has a marked positive anomaly of 6 % for the period 1980-2010

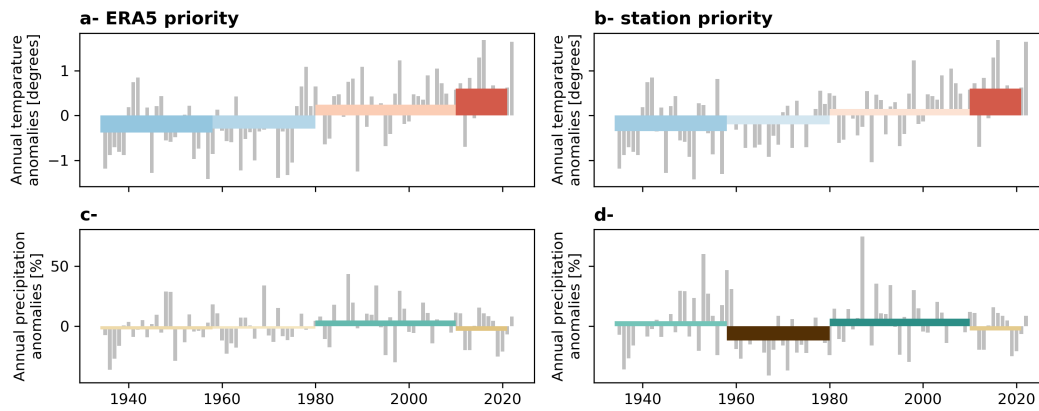


Fig. 7. Anomalies of temperature (a, b) and precipitation (c, d) for the "ERA5 priority" (a, c) and "station priority" (b, d) records. Colored boxes show the period considered in this study bounded by elevation data availability.

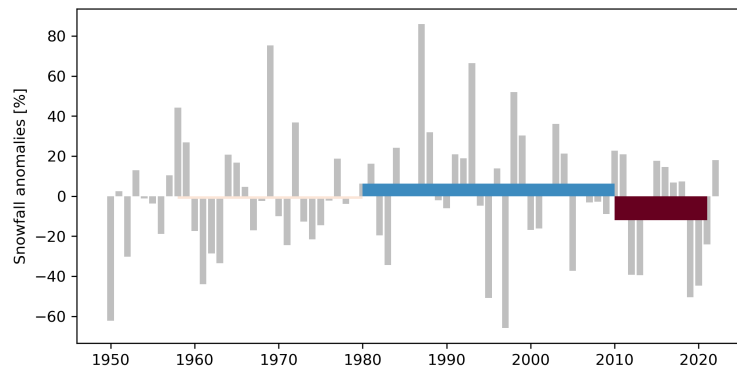


Fig. 8. Annual snowfall anomalies from ERA5 record

317 and a very negative anomaly of -12 % for the period 2011-2021, which is likely related to the positive
 318 temperature anomaly and might not be representative of what happens at higher elevation (Fig. 8).

319 DISCUSSION

320 Climate related elevation changes

321 Long-term elevation changes of Fedchenko Glacier are not homogeneous in time. While it is rather clear
 322 that the glacier has been thinning for almost a century (Lambrecht and others, 2014), our study allows
 323 to identify different patterns and rates of elevation changes for each sub-period that deciphers a complex
 324 glacier/climate relationship.

325 The earliest period is the one with the most limited changes of the glacier (from the terminus to 4600
 326 m elevation), with an average thinning of -0.27 m yr^{-1} (Table 3). The thinning is still significant, as well as

327 the tongue retreat, showing that the glacier was already out of equilibrium with climate. The limited data
328 collected above 4 600 m a.s.l show near zero elevation changes, meaning that the surface mass balance was
329 in equilibrium with the dynamics in the upper part of the glacier. This hints towards a slight disequilibrium
330 with climate, that could be an ongoing response of Fedchenko Glacier to the end of the little ice age, which
331 is estimated to culminate around 1600-1650 years AD in the Pamir Alay (Solomina, 2000).

332 A period of intense thinning between 1958 and 1975 for the glacier tongue was suspected by Zhou
333 and others (2019), because they found lower thinning rates for the period 1975–2000 than Lambrecht and
334 others (2014) for the period 1958–2000. Our study confirms their interpretation, as we find a mean rate of
335 elevation change of -0.77 m yr^{-1} over the shared area for the period 1958-1980. In terms of climatic record,
336 the station data show rather dry conditions (anomaly of -10%) during this period (Fig. 7), however, this
337 is not reflected in the ERA5 record (Fig. 7). The period 1968–1980 corresponds to negative ($-0.52 \pm$
338 $0.14 \text{ m w.e. a}^{-1}$) mass balance for Abramov Glacier located in the Pamir Alay, 90 km north of Fedchenko
339 Glacier front (Barandun and others, 2015; Kronenberg and others, 2022), which indicates that mass balance
340 conditions in the region were unfavourable during this time. Thinning in the upper area also suggest dry
341 conditions. Still, the pattern of thinning of the tongue for the period 1958-1980 is difficult to explain by a
342 climatic signal only (see the following discussion section).

343 The period 1980–2010 corresponds to moderate thinning, and even some slight thickening in the upper
344 area of Fedchenko Glacier (Table 3 and Fig. 4). Moderate glacier mass losses and slight mass gains can be
345 interpreted within the general picture of the "Karakoram anomaly" (Gardelle and others, 2012; Farinotti
346 and others, 2020). This anomaly of positive glacier mass balance is quite well documented for the central
347 Pamir in the beginning of the twenty-first century (Zhu and others, 2018; Lin and others, 2017; Holzer
348 and others, 2015; Brun and others, 2017; Shean and others, 2020), but there is no definitive conclusion
349 about its specific drivers (de Kok and others, 2018; Farinotti and others, 2020). From the ERA5 and
350 station data, it seems that this period corresponds to a wet anomaly (Fig. 7) that led to increased snowfall
351 (Fig. 8). Despite a positive temperature trend and anomaly, the excess precipitation and snowfall might
352 have mitigated the impact of rising temperature, and thus delayed the glaciers' response to this warming.
353 Moreover Fedchenko glacier lies in-between two well studied glaciers Abramov and Muztag Ata glaciers
354 that are sub-continental and continental types of glaciers, respectively. Fedchenko glacier is thus expected
355 to be also of continental/sub-continental type with a relatively low sensitivity to temperature changes (Zhu
356 and others, 2018; Wang and others, 2019; Arndt and Schneider, 2023; Wang and others, 2017).

357 The last period (2010–2021) is the period of most intense thinning, with a mean elevation change rate
358 of -0.79 m yr^{-1} . This is consistent with the largest positive temperature anomaly, and the slightly negative
359 precipitation anomaly that led to a large snowfall deficit (Fig. 8). The thinning is widespread, including in
360 the upper area of the glacier, where it reaches -0.31 m yr^{-1} , a number in agreement with previous studies
361 (Lambrecht and others, 2018). The most striking feature is the up-glacier propagation of thinning (Fig. 5).
362 It is noteworthy that this 11-yr period is shorter than the other ones, leading to higher uncertainties. The
363 intense thinning is consistent with the accelerating mass losses in high mountain Asia and the possible end
364 of the "Karakoram anomaly" (Hugonnet and others, 2021). The large snowfall anomaly of -12% for the
365 period 2011–2021 shows that there is also an impact of the rising rain-snow transition, because the snowfall
366 anomaly has a larger amplitude than the precipitation anomaly. The most recent thinning is thus likely a
367 combination of intensified melt and reduced accumulation, due to both a lack of precipitation and reduced
368 proportion of snow fall.

369 **A potential surge on Fedchenko main tongue?**

370 For the period 1958–1980, reduced precipitation should lead to generalised thinning, whereas the most
371 intense thinning happens only at the glacier tongue on the lowest 18 km (Fig. 4). Within two kilometers
372 the rates of thinning changes from -0.8 to -1.3 m yr^{-1} . Such a pattern suggests the implication of ice
373 dynamics as well, and potentially surge related mechanisms. Large thinning rates localised on glacier
374 tongues are frequently interpreted as post surge phases (e.g., Hewitt, 2007; Gardelle and others, 2012), but
375 this criteria is not sufficient to classify a glacier as surge-type. We thus searched for additional evidence to
376 support or to refute this interpretation.

377 The large thinning is located close to the confluence with the lowest tributary of Fedchenko Glacier,
378 Bivachny Glacier. This tributary is known for its past surges in 1976–78 and 2011–2015 (Kotlyakov and
379 others, 2008; Wendt and others, 2017). The surge of 1976–78 did not reach Fedchenko Glacier (Kotlyakov
380 and others, 2008). To our knowledge there is no documentation about earlier surges, which might have
381 reached Fedchenko main trunk as later surges did, like the 2011–15 surge (Wendt and others, 2017), and
382 impacted the rate of elevation changes on Fedchenko main trunk (Lambrecht and others, 2018). We
383 investigated the field reports from the late 50's but found no evidence of anomalous behaviour of Bivachny
384 Glacier.

385 We investigated images from the Corona KH-2, KH-4, KH-4B, and Hexagon KH-9 missions that were

386 acquired over the Pamirs from the sixties, until the eighties (Zhou and others, 2019; Goerlich and others,
387 2020; Ghuffar and others, 2022, Table 4). The orthoimage of 1968 is from Ghuffar and others (2022),
388 and the orthoimages of 1975 and 1980 are processed according to Dehecq and others (2020). The other
389 images are referenced using stable terrain features identified in the Pléiades orthoimage of 2021 and using
390 the *georeferencer* tool of QGIS. These images are thus not properly orthorectified, but simply registered,
391 leading to large uncertainties on the registration accuracy.

392 Visual inspection of the images reveals that downstream of the confluence with Bivachny Glacier, the
393 central part of Fedchenko tongue was much more crevassed in December 1960, than in the other years,
394 where it appears covered by debris, with distinct ice cliffs. Additionally, on its right side, Fedchenko Glacier
395 is touching the valley walls in December 1960 whereas the ice is approximately 100 m away from a deposited
396 moraine in August 1968 (Fig. 9). This observation suggests that parts of the thinning happened at the
397 beginning of the 1958-1980 period.

398 On the historical images, we also find the existence of a looped moraine on Fedchenko main trunk,
399 located close to the confluence with Bivachny Glacier in 1960 (Fig. 9). Looped moraines are common
400 features related to ice flow instabilities (Jennings and Hambrey, 2021). As the looped moraine is preserved
401 over two decades, we could track its location on the historical imagery (Figs. 9 and A7 and Table 4).
402 We assumed an uncertainty of 50 m on the location of the tip of the looped moraine, which is likely a
403 conservative estimate, especially for the most resolved images. The uncertainty in the displacement is thus
404 $\sqrt{2} * 50 = 71$ m, leading to uncertainties on the velocity that range from 12 to 23 m yr⁻¹.

405 The point scale velocity estimates from this method show that the 1962-1968 velocity is much larger
406 than all the other velocities estimated at this location, with 137 ± 12 m yr⁻¹ versus velocities from 65
407 ± 13 to 77 ± 23 m yr⁻¹ for the different periods from 1968 to 1980 (Table 4). The spatial variability of
408 the velocity cannot explain these differences, as the 2017-2018 velocity ranges from 49 to 79 m yr⁻¹ at
409 the location of the tip of the looped moraine (Table 4). The looped moraine is located in the vicinity of
410 the historical profile named profile X (Schulz, 1962), where velocity was measured by field techniques from
411 February 1958 until August 1959 (Fig. A7). The mean velocity along profile X for the period 1958-1959
412 is 26.7 cm d⁻¹, corresponding to 97.5 m yr⁻¹ (Schulz, 1962). Given that the looped moraine is located on
413 the side of the glacier, and given the present day observed profile, we can estimate that the velocity at the
414 looped moraine location is approximately 75% of the profile average velocity, which would lead to a velocity
415 of approximately 73 m yr⁻¹ in 1958-1959 (Fig. A7). This value is very close to the velocity estimates of the

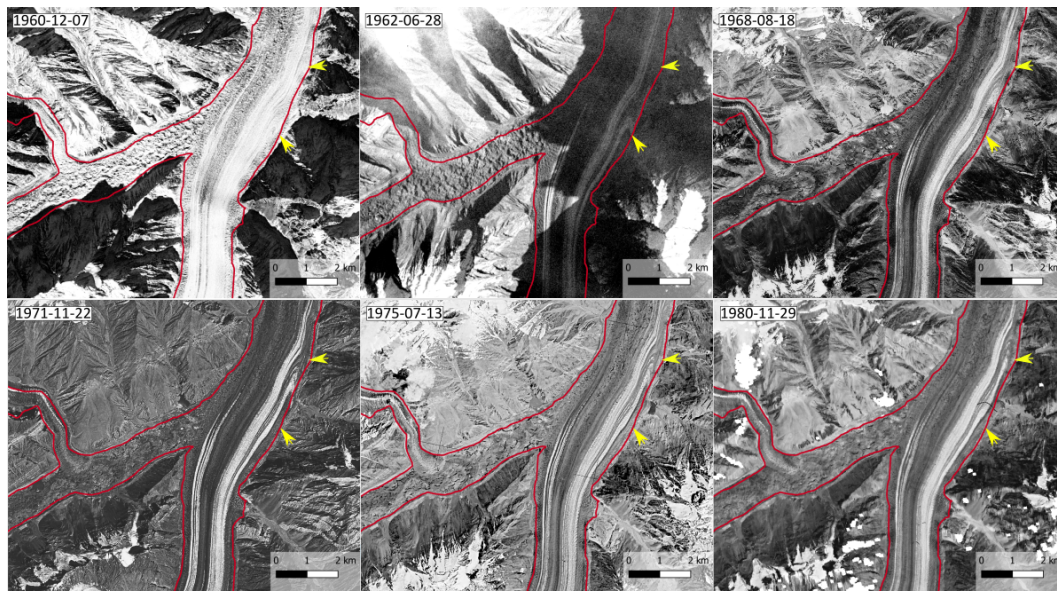


Fig. 9. Temporal evolution of a looped-moraine on Fedchenko main trunk, downstream of the confluence with Bivachny Glacier. Images: KH-4 and KH-9 series (Table 4). The yellow arrows are located at the same place on each image to help locating the looped-moraine and its displacement.

416 periods after 1968 (Table 4), but this very good agreement is to be taken with some caution, as we do not
 417 know exactly how the profile average velocities were measured in 1958-1959 (Schulz, 1962).

418 The analysis of velocities is still uncertain, but it indicates that the velocity close to the confluence
 419 with Bivachny was roughly twice as large between 1962 and 1968, than during all the other periods. We
 420 calculated a six year average that hides large temporal variability in velocity, and it is likely that the peak
 421 velocity was much larger. It is also noteworthy that this location of Fedchenko Glacier undergoes significant
 422 seasonal variability in velocity, with spring velocities being 50 % larger than annual averages, which might
 423 complicate the analysis (Nanni and others, 2023).

424 Given the qualitative and quantitative evidence gathered here, we can conclude that we suspect an
 425 internal surge, or at least a large speed-up, of Fedchenko main tongue that happened sometimes between
 426 August 1959 and August 1968. The mechanisms that led to this acceleration are completely unclear,
 427 but they might be related to pulses of meltwater originating from neighbouring surge-type glaciers. This
 428 acceleration did not lead to a front advance, nor to major flow disturbance, explaining why it was not
 429 noticed before. The specific surge inventories for the region investigated later periods (Goerlich and others,
 430 2020; Guillet and others, 2022; Guo and others, 2023). Given the extremely high density of surging glaciers
 431 in the surroundings, it is not very surprising to observe such kind of glacier flow instability.

Table 4. Additional images used to track the looped-moraine displacement. The values in between two lines represent the displacement of the tip of the looped-moraine and derived velocity between the two consecutive scenes. The present-day velocity is the velocity for 2017-2018 at the tip of the looped-moraine location extracted from Millan and others (2022). Figure A7 shows the locations of the tip of the looped-moraine for the different dates.

Date	Image ID	Mission	Disp. (m)	Velocity (m yr ⁻¹)	Present-day velocity (m yr ⁻¹)
1960-12-07	DS009013007DV168	KH-2			
1962-06-28	DS009038031AA024	KH-4			68
			841 ± 71	137 ± 12	
1968-08-18	DS1104-2169DF097	KH-4B			79
			237 ± 71	77 ± 23	
1971-09-21	DS1115-2169DA012	KH-4B			60
			282 ± 71	74 ± 19	
1975-07-13	DZB1210-500134L005001	KH-9			58
			347 ± 71	65 ± 13	
1980-11-29	DZB1216-500273L006001	KH-9			49

432 **The mystery of Jasgulem pass elevation changes**

433 Lambrecht and others (2014) already noticed a substantial thinning of more than 30 m for elevations above
 434 ~4700 m a.s.l. for the periods 1928-2000 and 1928-2009. Interestingly, they found that this thinning was
 435 increasing with increasing elevation. The data presented in this study show that the 2010-2021 pattern is
 436 opposite, with decreasing thinning rates with elevation (Fig. 5). Two previous hypotheses were proposed
 437 to explain the thinning: reduced accumulation, due to drier conditions that would lead to an imbalance
 438 between discharge and surface mass balance, and/or a densification of the firn due to increased temperature
 439 (Lambrecht and others, 2014). The second hypothesis is supported by observations of ice layers in the firn
 440 (Lambrecht and others, 2020), but can only partly explain the elevation changes, as the firn densification
 441 has a small impact on elevation changes (Ochwat and others, 2021).

442 The thinning is most pronounced downstream of Jasgulem pass (Fig. 10), an ice divide between ice
 443 flow towards Fedchenko Glacier (NE direction; Fig 1) and towards Jasgulem Glacier (SW direction). We
 444 report two intriguing features at Jasgulem pass. First, we observe a migration of the topographic divide,
 445 approximately 100 m towards Jasgulem between 1928 and 2019 (Fig. 10). The terrain is very flat, leading
 446 to high uncertainty on the location of the topographic divide, especially in the 1928 map. The divide

447 migration does not explain the thinning, but instead we observe that the shape of the elevation profile at
448 the divide location has changed (Fig. 10). In particular, we note that the past divide was more prominent,
449 with slightly steeper slopes within one kilometre in the downstream direction (Fig. 10).

450 Second, we also note that the ice flow divide location does not match with the topographic divide. We
451 identified the ice flow divide location by the minimum in the ice velocity (Millan and others, 2022), which is
452 located 1.4 km away from the topographic divide in direction of Jasgulem Glacier (Fig. 10). The location
453 of the ice flow divide is imposed by the bed geometry. Ground penetrating radar measurements show that
454 the glacier bed maximum elevation is not located at the topographic divide (Lambrecht and others, 2014,
455 2020, Fig. 10). Jasgulem Glacier is a surge-type glacier, with flow instabilities that are usually confined to
456 the lower elevations (Goerlich and others, 2020; Guo and others, 2023). It is thus unclear whether the ice
457 dynamics might impact the flow of Fedchenko glacier, due to their share the divide.

458 All the elements brought to this discussion point towards transient conditions at Jasgulem pass, but
459 we cannot make any definitive interpretation about the surprising features observed in this study.

460 **Uncertainties and limitations**

461 Our analysis relies heavily on the analysis of topographic data that originates from multiple sources (his-
462 torical ground photogrammetric surveys, spy satellite imagery, modern satellite imagery, satellite laser
463 altimetry and GNSS), each referring to different geodetic reference systems, which is particularly true
464 for the historical maps. Despite a careful processing of these data, it remains challenging to assess the
465 uncertainty in a quantitative way, due to the lack of stable terrain. We assessed the impact of the spa-
466 tial sampling in the method section, and found a moderate impact for the GNSS data, with a standard
467 deviation of 0.34 m, and a larger impact for ICESat data, with a standard deviation of 0.54 m. We also
468 assess the impact of the seasonal correction applied to the GNSS data. If we do not apply the correction,
469 we find rates of elevation changes 0.06 m yr^{-1} less negative for the period 2003-2009 and 0.11 m yr^{-1}
470 more negative for the 2016-2021 periods, respectively. These results correspond to a 25 % error, which
471 would change the interpretation of the results if not applied. The correction is based on only one period
472 of analysis in summer 2019, which is a limitation.

473 Providing highly accurate and spatially complete maps of elevation changes over large glaciers, such
474 as Fedchenko Glacier, is a challenge, even for the most recent sensors. DEMs from SAR sensors, such
475 as TanDEM-X allows covering large areas at once, and are thus well suited. However, they are impacted

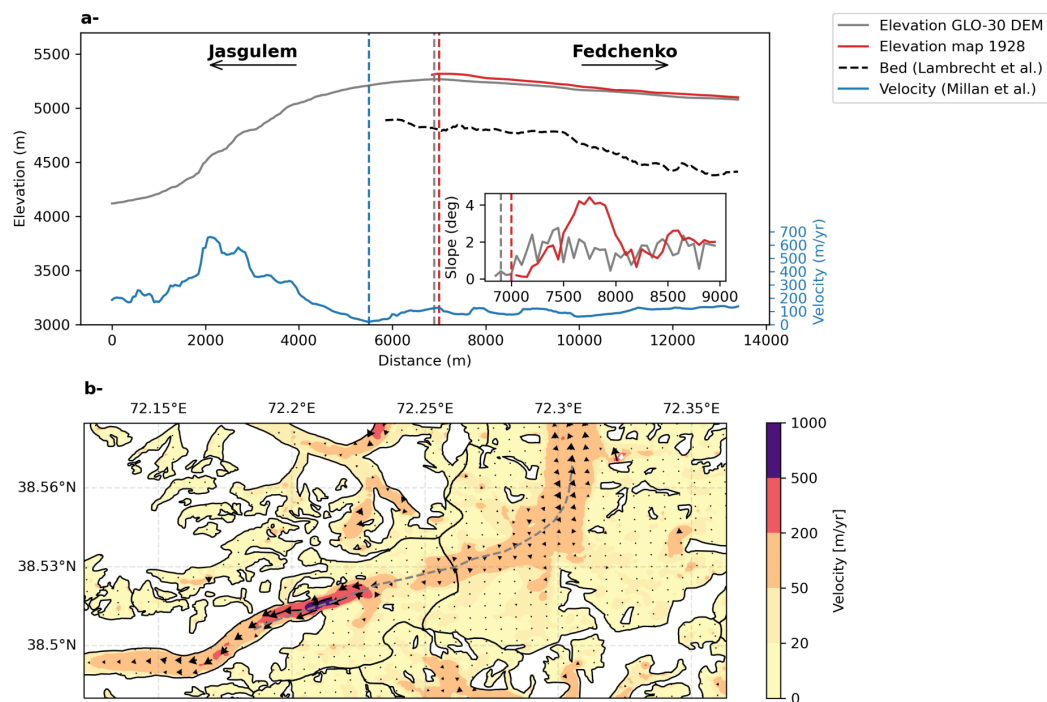


Fig. 10. Elevation and velocity along a 14 kilometre flow line crossing Jasgulem pass (a). The dashed vertical blue line show the minimum velocity (ice divide) and the dashed red and grey lines show the maximum elevation (topographic divide) in 1928 and in 2019, respectively. The Copernicus 30 m DEM (GLO-30DEM; European Space Agency, 2022) elevation is adjusted on the Pléiades 2019 elevation for consistency. The inset shows the slope within two kilometres along the flowline downstream of the topographic divide. The map (b) shows the surface velocity from Millan and others (2022) at the location of Jasgulem pass (solid black line separating the two main glaciers). The grey dashed line shows the flowline profile of panel a.

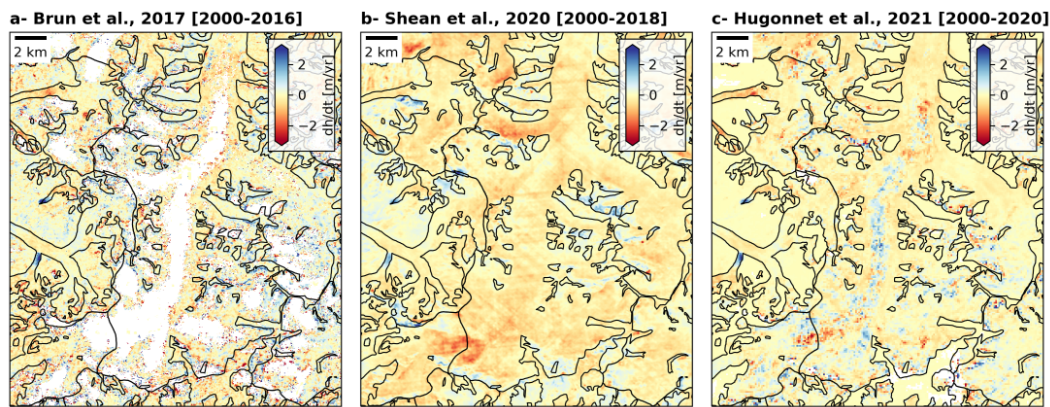


Fig. 11. Rates of elevation changes for the higher part of Fedchenko glacier from ASTER based studies (Brun and others, 2017; Shean and others, 2020; Hugonnet and others, 2021).

476 by the unknown penetration depth of the X-band signal (Li and others, 2021). For the specific case of
 477 Fedchenko Glacier, the X-band penetration is limited for September acquisitions for elevations below 5400
 478 m a.s.l. (Lambrecht and others, 2018). Time series of ASTER DEMs are also used to calculate geodetic
 479 mass balances, but the image correlation shows limited success in the high elevation areas, due to the lack
 480 of texture and/or the saturation of the images. This leads to artefacts or voids in the reconstructed DEMs,
 481 and thus to highly variable rates of elevation changes for three different studies (Fig. 11; Brun and others,
 482 2017; Shean and others, 2020; Hugonnet and others, 2021). Commercial optical sensors such as Pléiades or
 483 WorldView are less prone to saturation (Berthier and others, 2023), although it can still happen, as visible
 484 in the 1-2 August 2019 Pléiades DEM (Table 1). Thanks to their very high resolution (50 cm to 1 m of
 485 ground sampling distance) and radiometric depth, these sensors capture images with more texture than the
 486 lower resolution sensors. It is thus possible to derive void free DEMs on areas with limited or small surface
 487 features. The main limitation of these acquisitions is that they are commercial satellites, with limited user
 488 access to the tasking and to the existing archive. Another challenge is the limit of the swath width at 20
 489 km in the case of Pléiades, leading to acquisitions distributed over multiple days to cover a larger glacier
 490 such as Fedchenko (Table 1).

491 In this study we rely on ERA5 data to investigate the temporal changes in meteorological conditions.
 492 Barandun and Pohl (2023) showed that relying on different meteorological reanalysis can have an impact on
 493 the relative importance of the predictors of glacier mass balance variability. As ERA5 monthly estimates
 494 of temperature, and to a lesser extent precipitation, are in good agreement with the Fedchenko station
 495 measurements, we did not investigate other data sources, but it is clear that our analysis could benefit

496 from long-term climate simulations that cover the twentieth century.

497 CONCLUSION

498 In this study, we document more than nine decades of elevation changes of Fedchenko Glacier from 1928
499 to 2021, in the heart of the data scarce Central Pamir. We use various data sources, including topographic
500 maps, DEMs from optical satellites and GNSS surveys, allowing us to study four distinct sub-periods (1928-
501 1958, 1958-1980, 1980-2010, 2010-2021). These topographic data are combined with meteorological data
502 from Gorbunov Station (1936-1994) and ERA5 (1950-2021). Overall, we observe an up-glacier propagation
503 of the thinning rates, that are the largest for the most recent period of observation (2010-2021). In
504 particular, thinning rates of the accumulation basin reach -0.41 m yr^{-1} for the period 2016-2021. For some
505 periods it is possible to link the glacier rate of elevation change to climate anomalies. The period 1980-2010
506 shows limited thinning, and even thickening in the accumulation area. This periods corresponds to a wet
507 anomaly that might have limited mass loss. Still, the temporal variability in the rates of elevation changes
508 cannot be fully linked to the climate variability. For instance, for the period 1958-1980, we observe large
509 thinning on the tongue of Fedchenko Glacier that seems to be link to anomalously high velocities. This
510 example shows the limitation of relying on non complete maps of elevation changes to investigate glacier
511 mass changes.

512 ACKNOWLEDGEMENTS

513 We thank Sajid Ghuffar for sharing the 1968 Corona KH-4 orthoimage and DEM. EB acknowledges support
514 from the French Space Agency (CNES).

515 REFERENCES

- 516 Arndt A and Schneider C (2023) Spatial pattern of glacier mass balance sensitivity to atmospheric forcing in High
517 Mountain Asia. *Journal of Glaciology*, 1–18 (doi: 10.1017/jog.2023.46)
- 518 Barandun M and Pohl E (2023) Central Asia's spatiotemporal glacier response ambiguity due to data inconsistencies
519 and regional simplifications. *The Cryosphere*, **17**(3), 1343–1371, ISSN 1994-0416 (doi: 10.5194/tc-17-1343-2023)
- 520 Barandun M, Huss M, Sold L, Farinotti D, Azisov E, Salzmann N, Usabaliev R, Merkushkin A and Hoelzle M (2015)
521 Re-analysis of seasonal mass balance at Abramov glacier 1968-2014. *Journal of Glaciology*, **61**, 1103–1117 (doi:
522 10.3189/2015JoG14J239)

- 523 Berthier E, Arnaud Y, Kumar R, Ahmad S, Wagnon P and Chevallier P (2007) Remote sensing estimates of glacier
524 mass balances in the Himachal Pradesh (Western Himalaya, India). *Remote Sensing of Environment*, **108**(3),
525 327–338, ISSN 0034-4257 (doi: 10.1016/j.rse.2006.11.017)
- 526 Berthier E, Floriciou D, Gardner AS, Gourmelen N, Jakob L, Paul F, Treichler D, Wouters B, Belart JMC, Dehecq
527 A, Dussaillant I, Hugonnet R, Kääb A, Krieger L, Pálsson F and Zemp M (2023) Measuring glacier mass changes
528 from space—a review. *Reports on Progress in Physics*, **86**(3), 036801 (doi: 10.1088/1361-6633/acaf8e)
- 529 Berthier E, Lebreton J, Fontannaz D, Hosford S, Belart JMC, Brun F, Andreassen LM, Menounos B and Blondel C
530 (2024) The Pléiades Glacier Observatory: high resolution digital elevation models and ortho-imagery to monitor
531 glacier change. *EGUsphere*, **2024**, 1–25 (doi: 10.5194/egusphere-2024-250)
- 532 Beyer RA, Alexandrov O and McMichael S (2018) The Ames Stereo Pipeline: NASA’s Open Source Software for
533 Deriving and Processing Terrain Data. *Earth and Space Science*, **5**(9), 537–548, ISSN 2333-5084
- 534 Bhattacharya A, Bolch T, Mukherjee K, King O, Menounos B, Kapitsa V, Neckel N, Yang W and Yao T (2021)
535 High Mountain Asian glacier response to climate revealed by multi-temporal satellite observations since the 1960s.
536 *Nature Communications*, **12**(1), 4133, ISSN 2041-1723 (doi: 10.1038/s41467-021-24180-y)
- 537 Brun F, Berthier E, Wagnon P, Kääb A and Treichler D (2017) A spatially resolved estimate of High Mountain Asia
538 glacier mass balances from 2000 to 2016. *Nature Geoscience*, **10**, 668–673, ISSN 1752-0908 (doi: 10.1038/ngeo2999)
- 539 de Kok RJ, Tuinenburg OA, Bonekamp PNJ and Immerzeel WW (2018) Irrigation as a Potential Driver
540 for Anomalous Glacier Behavior in High Mountain Asia. *Geophysical Research Letters*, **45**, 2047–2054 (doi:
541 10.1002/2017GL076158)
- 542 Dehecq A, Millan R, Berthier E, Gourmelen N, Trouvé E and Vionnet V (2016) Elevation Changes Inferred From
543 TanDEM-X Data Over the Mont-Blanc Area: Impact of the X-Band Interferometric Bias. *IEEE Journal of Selected*
544 *Topics in Applied Earth Observations and Remote Sensing*, **9**(8), 3870–3882, ISSN 1939-1404 (doi: 10.1109/JS-
545 TARS.2016.2581482)
- 546 Dehecq A, Gardner AS, Alexandrov O, McMichael S, Hugonnet R, Shean D and Marty M (2020) Automated Process-
547 ing of Declassified KH-9 Hexagon Satellite Images for Global Elevation Change Analysis Since the 1970s. *Frontiers*
548 *in Earth Science*, **8**, 516, ISSN 2296-6463 (doi: 10.3389/feart.2020.566802)
- 549 Deschamps-Berger C, Gascoin S, Berthier E, Deems J, Gutmann E, Dehecq A, Shean D and Dumont M (2020) Snow
550 depth mapping from stereo satellite imagery in mountainous terrain: evaluation using airborne lidar data. *The*
551 *Cryosphere Discussions*, **2020**, 1–28 (doi: 10.5194/tc-2020-15)

- 552 Dittrich G (1964) *Geodätische Arbeiten im Rahmen der Glaziologischen Expedition der Usbekischen Akademie*
553 *der Wissenschaften zum Fedtschenkogletscher im Jahre 1958: Bericht der Teilnehmergruppe der Deutschen*
554 *Demokratischen Republik*. (Nationalkomitee für Geodäsie u. Geophysik d. Dt. Demokrat. Republ. bei d. Dt.
555 Akad. d. Wiss. zu Berlin, Fachgruppe Geodäsie), Nationalkomitee für Geodäsie und Geophysik der Deutschen
556 Demokratischen Republik bei der Deutschen Akademie der Wissenschaften
- 557 European Space Agency (2022) Copernicus DEM (doi: 10.5270/esa-c5d3d65)
- 558 Farinotti D, Immerzeel WW, de Kok RJ, Quincey DJ and Dehecq A (2020) Manifestations and mechanisms of the
559 Karakoram glacier Anomaly. *Nature Geoscience*, **13**(1), 8–16, ISSN 1752-0908 (doi: 10.1038/s41561-019-0513-5)
- 560 Finsterwalder R, Nöth L, Reinig W, Ficker H, Rickmers W and der Deutschen Wissenschaft N (1932) *Wis-*
561 *senschaftliche Ergebnisse der Alai-Pamir Expedition 1928: Geodätische, topographische, und glaziologische Ergeb-*
562 *nisse, von Dr. Richard Finsterwalder*. Wissenschaftliche Ergebnisse der Alai-Pamir Expedition 1928: im Auftrage
563 der Notgemeinschaft der deutschen Wissenschaft, D. Reimer/E. Vohsen
- 564 Gardelle J, Berthier E and Arnaud Y (2012) Slight mass gain of Karakoram glaciers in the early twenty-first century.
565 *Nature geoscience*, **5**(5), 322–325
- 566 Gardelle J, Berthier E, Arnaud Y and Käab A (2013) Region-wide glacier mass balances over the Pamir-Karakoram-
567 Himalaya during 1999-2011. *The Cryosphere*, **7**(4), 1263–1286 (doi: 10.5194/tc-7-1263-2013)
- 568 Ghuffar S, Bolch T, Rupnik E and Bhattacharya A (2022) A Pipeline for Automated Processing of Declassified
569 Corona KH-4 (1962–1972) Stereo Imagery. *IEEE Transactions on Geoscience and Remote Sensing*, **60**, 1–14 (doi:
570 10.1109/TGRS.2022.3200151)
- 571 Goerlich F, Bolch T and Paul F (2020) More dynamic than expected: an updated survey of surging glaciers in the
572 Pamir. *Earth System Science Data*, **12**(4), 3161–3176 (doi: 10.5194/essd-12-3161-2020)
- 573 Guillet G, King O, Lv M, Ghuffar S, Benn D, Quincey D and Bolch T (2022) A regionally resolved inventory of High
574 Mountain Asia surge-type glaciers, derived from a multi-factor remote sensing approach. *The Cryosphere*, **16**(2),
575 603–623 (doi: 10.5194/tc-16-603-2022)
- 576 Guo L, Li J, Dehecq A, Li Z, Li X and Zhu J (2023) A new inventory of High Mountain Asia surging glaciers derived
577 from multiple elevation datasets since the 1970s. *Earth System Science Data*, **15**(7), 2841–2861, ISSN 1866-3508
578 (doi: 10.5194/essd-15-2841-2023)
- 579 Hersbach H, Bell B, Berrisford P, Hirahara S, Horányi A, Muñoz-Sabater J, Nicolas J, Peubey C, Radu R and
580 Schepers D (2020) The ERA5 global reanalysis. *Quarterly Journal of the Royal Meteorological Society*, **146**(730),
581 1999–2049 (doi: 10.1002/qj.3803)

- 582 Hewitt K (2007) Tributary glacier surges: an exceptional concentration at Panmah Glacier, Karakoram Himalaya.
583 *Journal of Glaciology*, **53**(181), 181–188, ISSN 0022-1430 (doi: 10.3189/172756507782202829)
- 584 Hoelzle M, Azisov E, Barandun M, Huss M, Farinotti D, Gafurov A, Hagg W, Kenzhebaev R, Kronenberg M,
585 Machguth H, Merkushkin A, Moldobekov B, Petrov M, Saks T, Salzmann N, Schöne T, Tarasov Y, Usabaliev R,
586 Vorogushyn S, Yakovlev A and Zemp M (2017) Re-establishing glacier monitoring in Kyrgyzstan and Uzbekistan,
587 Central Asia. *Geoscientific Instrumentation, Methods and Data Systems*, **6**(2), 397–418 (doi: 10.5194/gi-6-397-
588 2017)
- 589 Holzer N, Vijay S, Yao T, Xu B, Buchroithner M and Bolch T (2015) Four decades of glacier variations at Muztagh
590 Ata (eastern Pamir): a multi-sensor study including Hexagon KH-9 and Pléiades data. *The Cryosphere*, **9**(6),
591 2071–2088 (doi: 10.5194/tc-9-2071-2015)
- 592 Hugonnet R, McNabb R, Berthier E, Menounos B, Nuth C, Girod L, Farinotti D, Huss M, Dussaillant I, Brun F and
593 Kääh A (2021) Accelerated global glacier mass loss in the early twenty-first century. *Nature*, **592**(7856), 726–731,
594 ISSN 1476-4687 (doi: 10.1038/s41586-021-03436-z)
- 595 Hugonnet R, Brun F, Berthier E, Dehecq A, Mannerfelt ES, Eckert N and Farinotti D (2022) Uncertainty analysis
596 of digital elevation models by spatial inference from stable terrain. *IEEE Journal of Selected Topics in Applied*
597 *Earth Observations and Remote Sensing*, 1–17 (doi: 10.1109/JSTARS.2022.3188922)
- 598 Immerzeel WW, Lutz AF, Andrade M, Bahl A, Biemans H, Bolch T, Hyde S, Brumby S, Davies BJ, Elmore AC,
599 Emmer A, Feng M, Fernández A, Haritashya U, Kargel JS, Koppes M, Kraaijenbrink PDA, Kulkarni AV, Mayewski
600 PA, Nepal S, Pacheco P, Painter TH, Pellicciotti F, Rajaram H, Rupper S, Sinisalo A, Shrestha AB, Viviroli D,
601 Wada Y, Xiao C, Yao T and Baillie JEM (2020) Importance and vulnerability of the world’s water towers. *Nature*,
602 **577**(7790), 364–369, ISSN 1476-4687 (doi: 10.1038/s41586-019-1822-y)
- 603 Jennings SJA and Hambrey MJ (2021) Structures and Deformation in Glaciers and Ice Sheets. *Reviews of Geophysics*,
604 **59**(3), e2021RG000743, ISSN 1944-9208
- 605 Khadka A, Wagnon P, Brun F, Shrestha D, Lejeune Y and Arnaud Y (2022) Evaluation of ERA5-Land and HARv2
606 Reanalysis Data at High Elevation in the Upper Dudh Koshi Basin (Everest Region, Nepal). *Journal of Applied*
607 *Meteorology and Climatology*, **61**(8), 931 – 954 (doi: 10.1175/JAMC-D-21-0091.1)
- 608 Korona J, Berthier E, Bernard M, Rémy F and Thouvenot E (2009) SPIRIT. SPOT 5 stereoscopic survey of Polar
609 Ice: Reference Images and Topographies during the fourth International Polar Year (2007-2009). *ISPRS Journal*
610 *of Photogrammetry and Remote Sensing*, **64**, 204–212 (doi: 10.1016/j.isprsjprs.2008.10.005)
- 611 Kotlyakov VM, Osipova GB and Tsvetkov DG (2008) Monitoring surging glaciers of the Pamirs, central Asia, from
612 space. *Annals of Glaciology*, **48**, 125–134, ISSN 0260-3055, 1727-5644 (doi: 10.3189/172756408784700608)

- 613 Kronenberg M, Machguth H, Eichler A, Schwikowski M and Hoelzle M (2021) Comparison of historical and recent
614 accumulation rates on Abramov Glacier, Pamir Alay. *Journal of Glaciology*, **67**(262), 253–268, ISSN 0022-1430
615 (doi: 10.1017/jog.2020.103)
- 616 Kronenberg M, van Pelt W, Machguth H, Fiddes J, Hoelzle M and Pertziger F (2022) Long-term firn and mass
617 balance modelling for Abramov Glacier in the data-scarce Pamir Alay. *The Cryosphere*, **16**(12), 5001–5022 (doi:
618 10.5194/tc-16-5001-2022)
- 619 Kääb A, Berthier E, Nuth C, Gardelle J and Arnaud Y (2012) Contrasting patterns of early twenty-first-century
620 glacier mass change in the Himalayas. *Nature*, **488**(7412), 495–498 (doi: 10.1038/nature11324)
- 621 Lambrecht A, Mayer C, Aizen V, Floricioiu D and Surazakov A (2014) The evolution of Fedchenko glacier
622 in the Pamir, Tajikistan, during the past eight decades. *Journal of Glaciology*, **60**(220), 233–244 (doi:
623 10.3189/2014JoG13J110)
- 624 Lambrecht A, Mayer C, Wendt A, Floricioiu D and Völksen C (2018) Elevation change of Fedchenko Glacier, Pamir
625 Mountains, from GNSS field measurements and TanDEM-X elevation models, with a focus on the upper glacier.
626 *Journal of Glaciology*, **64**(246), 637–648 (doi: 10.1017/jog.2018.52)
- 627 Lambrecht A, Mayer C, Bohleber P and Aizen V (2020) High altitude accumulation and preserved climate information
628 in the western Pamir, observations from the Fedchenko Glacier accumulation basin. *Journal of Glaciology*, **66**(256),
629 219–230 (doi: 10.1017/jog.2019.97)
- 630 Li J, Li ZW, Hu J, Wu LX, Li X, Guo L, Liu Z, Miao ZL, Wang W and Chen JL (2021) Investigating the bias
631 of TanDEM-X digital elevation models of glaciers on the Tibetan Plateau: impacting factors and potential ef-
632 fects on geodetic mass-balance measurements. *Journal of Glaciology*, **67**(264), 613–626, ISSN 0022-1430 (doi:
633 10.1017/jog.2021.15)
- 634 Lin H, Li G, Cuo L, Hooper A and Ye Q (2017) A decreasing glacier mass balance gradient from the edge of the
635 Upper Tarim Basin to the Karakoram during 2000–2014. *Scientific Reports*, **7**(1), 6712, ISSN 2045-2322 (doi:
636 10.1038/s41598-017-07133-8)
- 637 Machguth H, Eichler A, Schwikowski M, Brüttsch S, Mattea E, Kutuzov S, Heule M, Usabaliev R, Belevkov S,
638 Mikhailenko VN, Hoelzle M and Kronenberg M (2024) Fifty years of firn evolution on Grigoriev ice cap, Tien Shan,
639 Kyrgyzstan. *The Cryosphere*, **18**(4), 1633–1646 (doi: 10.5194/tc-18-1633-2024)
- 640 Miles E, McCarthy M, Dehecq A, Kneib M, Fugger S and Pellicciotti F (2021) Health and sustainability of glaciers
641 in High Mountain Asia. *Nature Communications*, **12**(1), 2868, ISSN 2041-1723 (doi: 10.1038/s41467-021-23073-4)

- 642 Millan R, Mouginot J, Rabatel A and Morlighem M (2022) Ice velocity and thickness of the world's glaciers. *Nature*
643 *Geoscience*, **15**(2), 124–129, ISSN 1752-0908 (doi: 10.1038/s41561-021-00885-z)
- 644 Nanni U, Scherler D, Ayoub F, Millan R, Herman F and Avouac JP (2023) Climatic control on seasonal variations
645 in mountain glacier surface velocity. *The Cryosphere*, **17**(4), 1567–1583, ISSN 1994-0416 (doi: 10.5194/tc-17-1567-
646 2023)
- 647 Nuth C and Kääb A (2011) Co-registration and bias corrections of satellite elevation data sets for quantifying glacier
648 thickness change. *The Cryosphere*, **5**(1), 271–290 (doi: 10.5194/tc-5-271-2011)
- 649 Ochwat NE, Marshall SJ, Moorman BJ, Criscitiello AS and Copland L (2021) Evolution of the firn pack of Kaskawulsh
650 Glacier, Yukon: meltwater effects, densification, and the development of a perennial firn aquifer. *The Cryosphere*,
651 **15**(4), 2021–2040 (doi: 10.5194/tc-15-2021-2021)
- 652 Orsolini Y, Wegmann M, Dutra E, Liu B, Balsamo G, Yang K, de Rosnay P, Zhu C, Wang W, Senan R and Arduini
653 G (2019) Evaluation of snow depth and snow cover over the Tibetan Plateau in global reanalyses using in situ and
654 satellite remote sensing observations. *The Cryosphere*, **13**(8), 2221–2239 (doi: 10.5194/tc-13-2221-2019)
- 655 Pritchard HD (2019) Asia's shrinking glaciers protect large populations from drought stress. *Nature*, **569**(7758),
656 649–654, ISSN 1476-4687 (doi: 10.1038/s41586-019-1240-1)
- 657 RGI Consortium (2023) Randolph Glacier Inventory - A Dataset of Global Glacier Outlines, Version 7 (doi:
658 10.5067/F6JMOVY5NAVZ)
- 659 Rignot E, Echelmeyer K and Krabill W (2001) Penetration depth of interferometric synthetic-aperture radar signals
660 in snow and ice. *Geophysical Research Letters*, **28**, 3501–3504 (doi: 10.1029/2000GL012484)
- 661 Rolstad C, Haug T and Denby B (2009) Spatially integrated geodetic glacier mass balance and its uncertainty based
662 on geostatistical analysis: application to the western Svartisen ice cap, Norway. *Journal of Glaciology*, **55**(192),
663 666–680 (doi: 10.3189/002214309789470950)
- 664 Schulz VL (1962) *Fedchenko Glacier*, volume 1. Academy of Sciences of Usbekistan, Tashkent
- 665 Shean DE, Bhushan S, Montesano P, Rounce DR, Arendt A and Osmanoglu B (2020) A Systematic, Regional
666 Assessment of High Mountain Asia Glacier Mass Balance. *Frontiers in Earth Science*, **7**, 363, ISSN 2296-6463 (doi:
667 10.3389/feart.2019.00363)
- 668 Solomina ON (2000) Retreat of mountain glaciers of northern Eurasia since the Little Ice Age maximum. *Annals of*
669 *Glaciology*, **31**, 26–30, ISSN 0260-3055, 1727-5644 (doi: 10.3189/172756400781820499)

- 670 Wang Q, Yi S and Sun W (2017) Precipitation-driven glacier changes in the Pamir and Hindu Kush mountains.
671 *Geophysical Research Letters*, **44**(6), 2017GL072646, ISSN 1944-8007 (doi: 10.1002/2017GL072646)
- 672 Wang R, Liu S, Shangguan D, Radić V and Zhang Y (2019) Spatial Heterogeneity in Glacier Mass-Balance Sensitivity
673 across High Mountain Asia. *Water*, **11**(4), ISSN 2073-4441 (doi: 10.3390/w11040776)
- 674 Wendt A, Mayer C, Lambrecht A and Floricioiu D (2017) A Glacier Surge of Bivachny Glacier, Pamir Mountains,
675 Observed by a Time Series of High-Resolution Digital Elevation Models and Glacier Velocities. *Remote Sensing*,
676 **9**(4), 388 (doi: 10.3390/rs9040388)
- 677 Williams MW and Konovalov VG (2008) Central Asia Temperature and Precipitation Data, 1879-2003, Version 1
678 (doi: 10.7265/N5NK3BZ8)
- 679 Zhou Y, Li Z, Li J, Zhao R and Ding X (2019) Geodetic glacier mass balance (1975-1999) in the central Pamir using
680 the SRTM DEM and KH-9 imagery. *Journal of Glaciology*, **65**, 309–320, ISSN 0022-1430 (doi: 10.1017/jog.2019.8),
681 aDS Bibcode: 2019JGlac..65..309Z
- 682 Zhu M, Yao T, Yang W, Xu B, Wu G, Wang X and Xie Y (2018) Reconstruction of the mass balance of Muz-
683 tag Ata No. 15 glacier, eastern Pamir, and its climatic drivers. *Journal of Glaciology*, **64**(244), 259–274 (doi:
684 10.1017/jog.2018.16)
- 685 Zwally H, Schutz B, Abdalati W, Abshire J, Bentley C, Brenner A, Bufton J, Dezio J, Hancock D, Harding
686 D, Herring T, Minster B, Quinn K, Palm S, Spinhirne J and Thomas R (2002) Icesat's laser measurements
687 of polar ice, atmosphere, ocean, and land. *Journal of Geodynamics*, **34**(3), 405–445, ISSN 0264-3707 (doi:
688 [https://doi.org/10.1016/S0264-3707\(02\)00042-X](https://doi.org/10.1016/S0264-3707(02)00042-X))

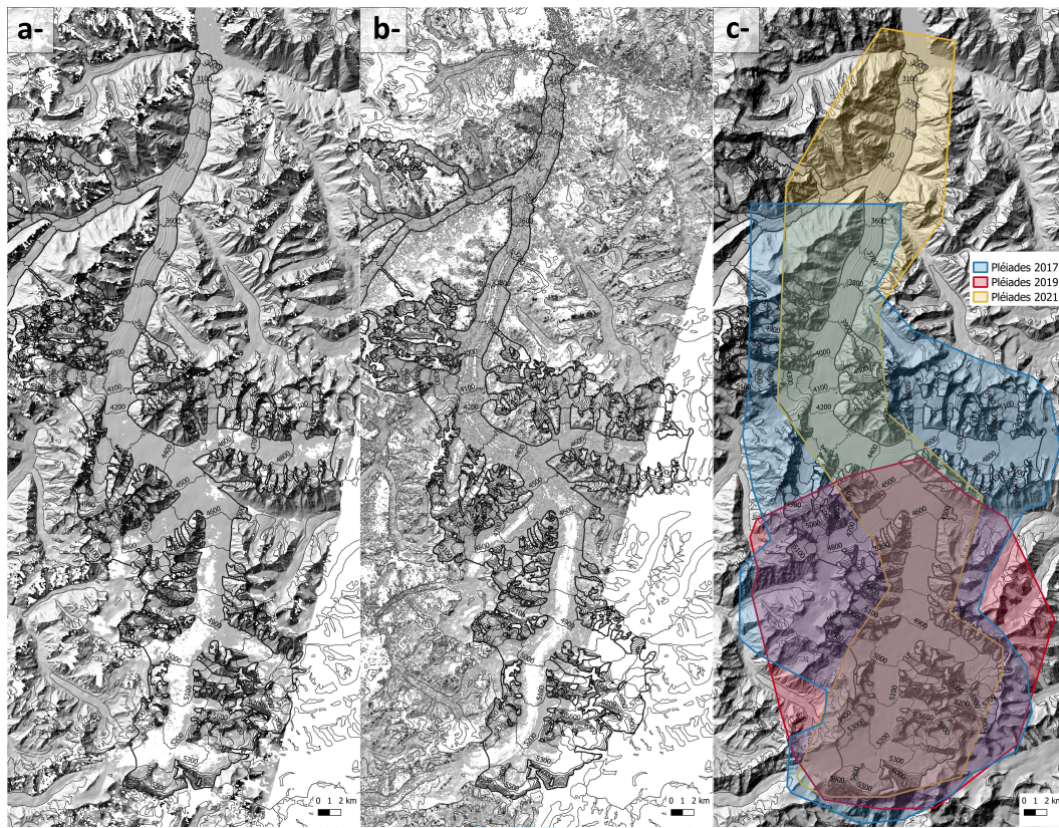


Fig. A1. Hillshades from the KH-9 (a) and SPOT 5 (b) DEMs. Panel c shows the footprint of the different Pléiades DEMs.

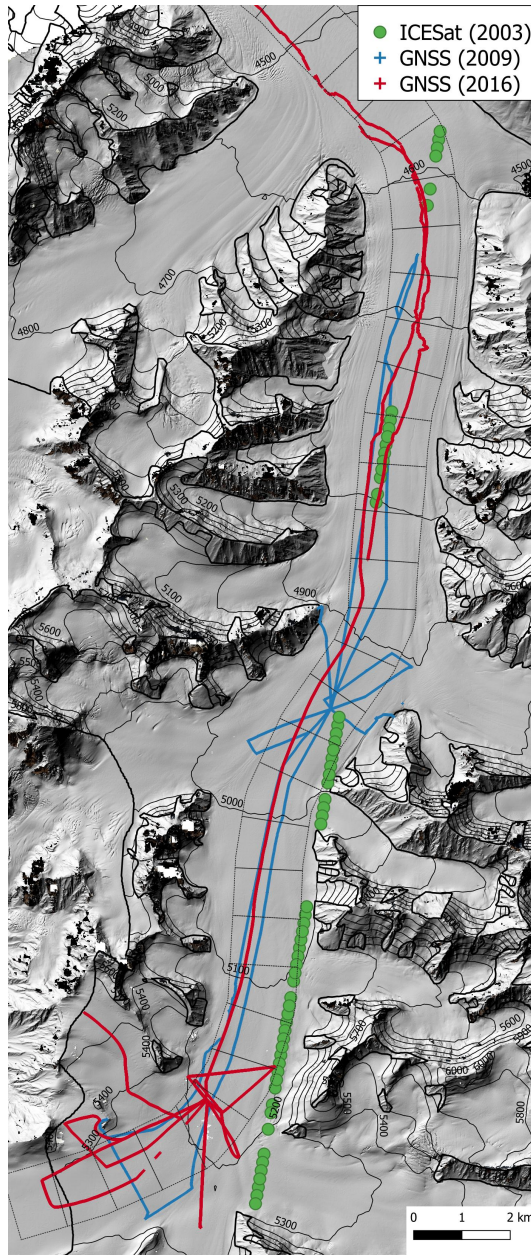


Fig. A2. Summary of the ICESat and GNSS acquisitions

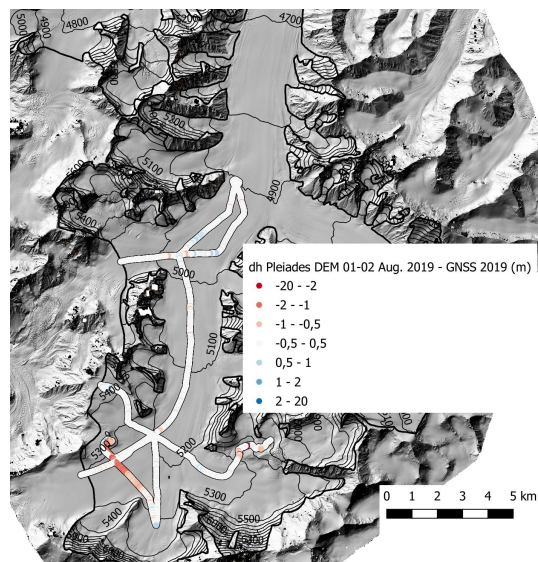


Fig. A3. Elevation difference between GNSS measurements and the average between the Pléiades DEMs of 1-2 and 28-29 August 2019 after co-registration. Note some spurious measurements in one GNSS track that was discarded from the analysis.



Fig. A4. Elevation difference between the Pléiades DEM of 22-23 September 2019 and the Pléiades DEM of 1-2 August 2019 that is used for the seasonal correction of GNSS data.

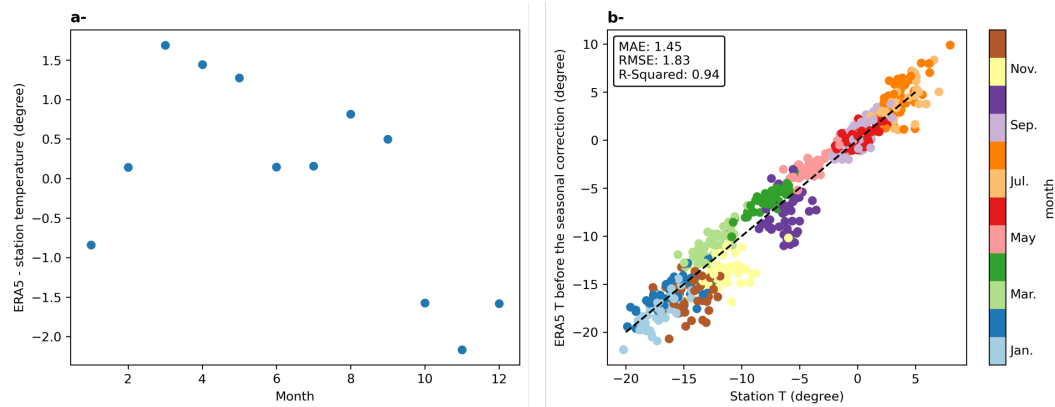


Fig. A5. Mean monthly temperature bias in ERA5 data (a) and monthly ERA5 versus the station temperature before seasonal bias correction (b).

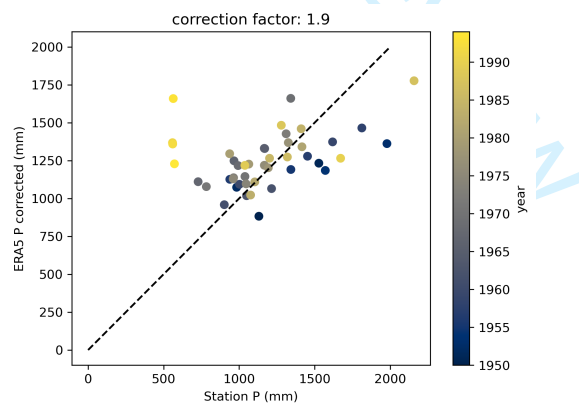


Fig. A6. Comparison of the annual ERA5 adjusted precipitation the annual station record for the overlapping years (1950-1994). Note the spurious values for the years 1990 to 1994 in the station record. These values were excluded from the analysis.

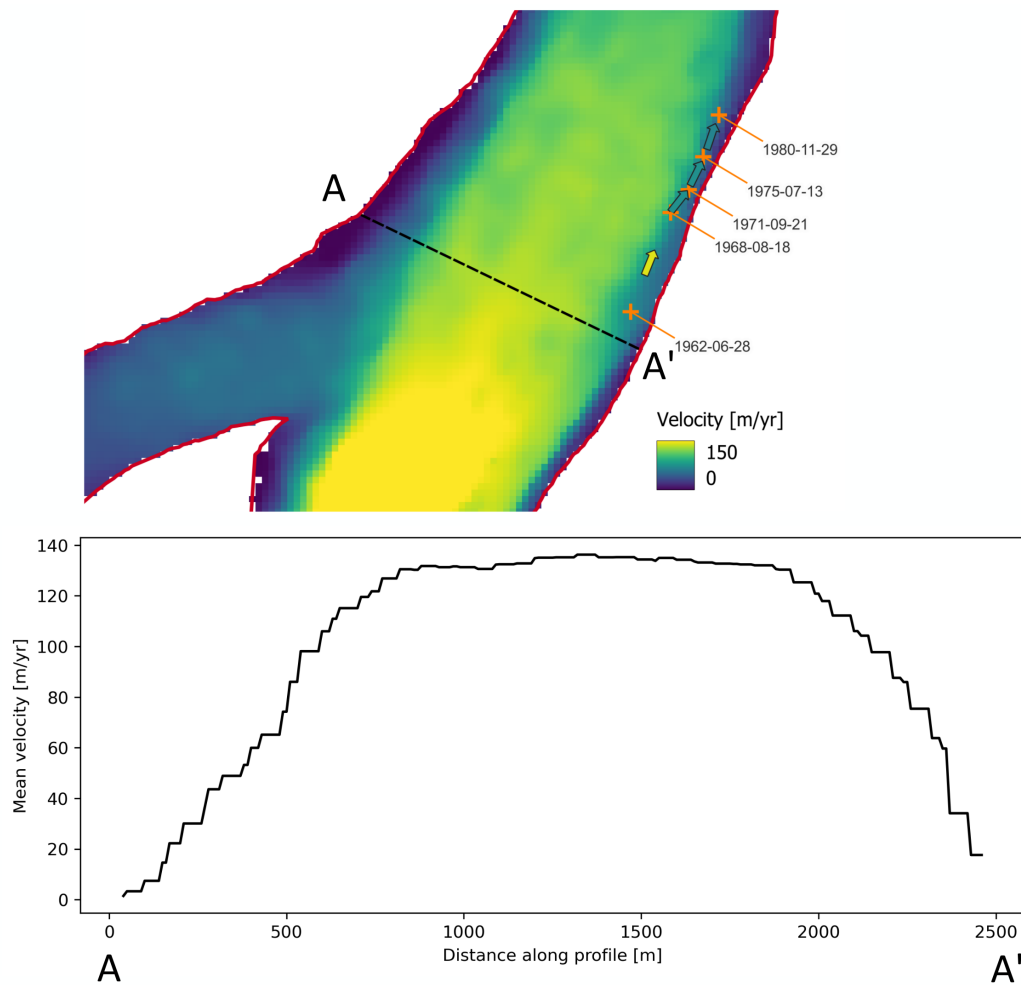


Fig. A7. Map of the location of the tip of the looped moraine identified in the spy satellite imagery (Table 4 and Fig. 9). The background is the velocity map from Millan and others (2022), and the arrows show the velocity inferred from the looped-moraine tracking. The graph shows the velocity profile along the AA' line (corresponding to the approximate location of the X profile) from Millan and others (2022).